A Tsunami Forecast Model for Pago Pago Harbor, American Samoa

Uslu, B.

List of Tables

List of figures

Maximum computed wave heights computed with forecast model grids. (c) Comparison of time series computed with reference model and forecast model grids at the Pago Pago tide gauge.

18. Magnitude 9.4 AASZ source segment 16-25 synthetic scenario model results. (a) Maximum computed wave heights computed with reference model grids. (b) Maximum computed wave heights computed with forecast model grids. (c) Comparison of time series computed with reference model and forecast model grids at the Pago Pago tide gauge.
19. Magnitude 9.4 AASZ source segment 22-31 synthetic scenario model results. (a) Maximum computed wave heights computed with reference model grids. (b) Maximum computed wave heights computed with forecast model grids. (c) Comparison of time series computed with reference model and forecast model grids at the Pago Pago tide gauge.
20. Magnitude 9.4 AASZ source segment 50-59 synthetic scenario model results. (a) Maximum computed wave heights computed with reference model grids. (b) Maximum computed wave heights computed with forecast model grids. (c) Comparison of time series computed with reference model and forecast model grids at the Pago Pago tide gauge.
21. Magnitude 9.4 AASZ source segment 56-65 synthetic scenario model results. (a) Maximum computed wave heights computed with reference model grids. (b) Maximum computed wave heights computed with forecast model grids. (c) Comparison of time series computed with reference model and forecast model grids at the Pago Pago tide gauge.
22. Magnitude 9.4 CSSZ source segment 1-10 synthetic scenario model results. (a) Maximum computed wave heights computed with reference model grids. (b) Maximum computed wave heights computed with forecast model grids. (c) Comparison of time series computed with reference model and forecast model grids at the Pago Pago tide gauge.
23. Magnitude 9.4 CSSZ source segment 37-46 synthetic scenario model results. (a) Maximum computed wave heights computed with reference model grids. (b) Maximum computed wave heights computed with forecast model grids. (c) Comparison of time series computed with reference model and forecast model grids at the Pago Pago tide gauge.
24. Magnitude 9.4 CSSZ source segment 89-98 synthetic scenario model results. (a) Maximum computed wave heights computed with reference model grids. (b) Maximum computed wave heights computed with forecast model grids. (c) Comparison of time series computed with reference model and forecast model grids at the Pago Pago tide gauge.
25. Magnitude 9.4 CSSZ source segment 102-111 synthetic scenario model results. (a) Maximum computed wave heights computed with reference model grids. (b) Maximum computed wave heights computed with forecast model grids. (c) Comparison of time series computed with reference model and forecast model grids at the Pago Pago tide gauge.
26. Magnitude 9.4 EPSZ source segment 6-15 synthetic scenario model results. (a) Maximum computed wave heights computed with reference model grids. (b) Maximum computed wave heights computed with forecast model grids. (c)

A Tsunami Forecast Model for Pago Pago Harbor, American Samoa

Uslu, B.

Table of Content

Abstract The National Oceanic and Atmospheric Administration has developed a tsunami forecast model for Pago Pago Harbor, American Samoa as part of an effort to provide tsunami forecasts for communities along vulnerable United States coastlines. The American Samoa is located on the Pacific Rim in a seismically active location. The local possible earthquakes and shallow complex geomorphology of the islands chain provide for a challenging environment in which to conduct tsunami research and forecast modeling. The tsunami disaster stemming from the great December 2004 Indian Ocean earthquake has provided an opportunity for investigating not previously available from the historical written record. In particular, this large–scale event has provided an opportunity to study the contribution of reefs and the deep trench to the wave dynamics. Even though 2009 Samoa earthquake brought up extra attention to the American Samoa and Pago Pago harbor, the region has experienced earthquakes from Kermadec Islands (1986, 1976), Fiji (1937, 1919) and Tonga (2009, 2006, 1919). This study assesses the hazard at the ports and harbors on the island of American Samoa from local and far-field earthquakes. A real–time wave forecast is suggested for the Pago Pago harbor because the governing dynamics are distinct from other Pacific Ocean regions. In addition, the location of American Samoa within the Pacific Ocean makes it vulnerable to both locally generated tsunamis and those that may not necessarily have Pacific wide

consequences and trans-oceanic as well. The results of this study suggest tsunami with a wave amplitude larger 4 m might be experienced in Samoa from a Mw 9.4 earthquake in Chile, Kuril Islands or Aleutians, which larger than it was in 2009 Samoa tsunami.

1.0 Background and Objectives

The National Oceanic and Atmospheric Administration (NOAA) Center for Tsunami Research (NCTR) at the NOAA Pacific Marine Environmental Laboratory (PMEL) has developed a tsunami forecasting capability for operational use by NOAA's two Tsunami Warning Centers located in Hawaii and Alaska (Titov *et al*., 2005). The system is designed to efficiently provide basin-wide warning of approaching tsunami waves accurately and quickly. The system, termed Short-term Inundation Forecast of Tsunamis (SIFT) combines real-time tsunami event data with numerical models to produce estimates of tsunami wave arrival times and amplitudes at a coastal community of interest. The SIFT system integrates several key components: deep-ocean observations of tsunamis in real-time, a basin-wide pre-computed propagation database of water level and flow velocities based on potential seismic unit sources, an inversion algorithm to refine the tsunami source based on deep ocean observations during an event, and high-resolution tsunami forecast models. Figure 1 shows the global network of tsunameters that continually monitor the world oceans and provide deep-ocean observations during tsunami propagation.

A tsunami inundation forecast model has been developed for Pago Pago Harbor, American Samoa. The low-lying community is vital to the island economy and to the interests of the United States militarily. The objective in developing this model is to provide NOAA's two Tsunami Warning Centers the ability to assess danger posed to the Harbor region following tsunami generation in the Pacific Ocean Basin with a goal to provide accurate and timely forecasts to enable the United States military and the civilian community to respond appropriately.

2.0 Forecast Methodology

A high-resolution inundation model was used as the basis for development of a tsunami forecast model to operationally provide an estimate of wave arrival time, wave height, and inundation at Apra Harbor, Guam following tsunami generation. All tsunami forecast models are run in real time while a tsunami is propagating across the open ocean. The Apra Harbor model was designed and tested to perform under stringent time constraints given that time is generally the single limiting factor in saving lives and property. The goal of this work is to maximize the length of time that the community of Apra Harbor has to react to a tsunami threat by providing accurate information quickly to emergency managers and other officials responsible for the community and infrastructure.

The general tsunami forecast model, based on the Method of Splitting Tsunami (MOST), is used in the tsunami inundation and forecasting system to provide real-time tsunami

forecasts at selected coastal communities. The model runs in minutes while employing high-resolution grids constructed by the Pacific Marine Environmental Laboratory. The Method of Splitting Tsunami (MOST) is a suite of numerical simulation codes capable of simulating three processes of tsunami evolution: earthquake, transoceanic propagation, and inundation of dry land. The MOST model has been extensively tested against a number of laboratory experiments and benchmarks (Synolakis *et al.*, 2008) and was successfully used for simulations of many historical tsunami events. The main objective of a forecast model is to provide an accurate, yet rapid, estimate of wave arrival time, wave height, and inundation in the minutes following a tsunami event. Titov and González (1997) describe the technical aspects of forecast model development, stability, testing, and robustness, and Tang *et al*., 2009 provide detailed forecast methodology.

A basin-wide database of pre-computed water elevations and flow velocities for unit sources covering worldwide subduction zones has been generated to expedite forecasts (Gica *et al.*, 2008). As the tsunami wave propagates across the ocean and successively reaches tsunameter observation sites, recorded sea level is ingested into the tsunami forecast application in near real-time and incorporated into an inversion algorithm to produce an improved estimate of the tsunami source. A linear combination of the pre-computed database is then performed based on this tsunami source, a source that reflects the transfer of energy to the fluid body and thus a transfer of the governing physics from earth to ocean, to produce synthetic boundary conditions of water elevation and flow velocities to initiate the forecast model computation.

Accurate forecasting of the tsunami impact on Pago Pago, American Samoa largely relies on the accuracies of bathymetry and topography and the numerical computation. The high spatial and temporal grid resolution necessary for modeling accuracy poses a challenge in the run-time requirement for real-time forecasts. Each forecast model consists of three telescoped grids with increasing spatial resolution in the finest grid, and temporal resolution for simulation of wave inundation onto dry land. The forecast model utilizes the most recent bathymetry and topography available to reproduce the correct wave dynamics during the inundation computation. Forecast models, including the Seaside model, are constructed for at-risk populous coastal communities in the Pacific and Atlantic Oceans. Previous and present development of forecast models in the Pacific (Titov *et al*., 2005; Titov, 2009; Tang *et al*., 2008; Wei *et al*., 2008) have validated the accuracy and efficiency of each forecast model currently implemented in the real-time tsunami forecast system. Models are tested in real-time at every opportunity during an event and are used for scientific research. Tang *et al*., 2009 provide forecast methodology details.

3.0 Model Development

The methodology in developing the Pago Pago tsunami forecast model was to develop a set of three nested grids from a high-resolution digital elevation model provided by NOAA's National Geophysical Data Center (NGDC). High resolution grids for the Pago Pago Bay and its vicinity are constructed from the best available data referenced to Mean High Water, as shown in Figure 2. Afterwards, the Forecast Model grids are developed with reference high resolution grids optimized to run in an operationally specified period

of time, whereas the aim of the reference model is accuracy, but the forecast model is optimized to time efficient to be used operationally.

Referred to as A, B, and C, the three nested grids each become successively finer in resolution as they telescope into Pago Pago. Offshore Apra Harbor is covered by the largest and lowest resolution A-grid while the near-shore details are resolved within the finest scale C-grid to the point that tide gauge observations recorded during historical tsunamis are resolved within expected accuracy limits. The general procedure to develop the Pago Pago forecast model is to begin development with large spatial extent merged bathymetric topographic grids at high resolution, and then optimize these grids by sub sampling to coarsen the resolution and shrink the overall grid dimensions to achieve a 4 to 10 hr simulation of modeled tsunami waves within the required time period of 10 min of wall-clock time. The forecast model is developed by incrementally reducing the resolution and extent of the coverage of the reference model, as described in Tang et al. (2008). It is possible to develop 3 arc–sec fast–running optimized numerical grids that can predict time histories at desired numerical tide gauges with high accuracy (Tang et al., 2006).

3.1 Forecast area

The western influence in Samoa started with the first western exploration from Netherlands by Jacob Roggeveen, in 1772 (Samoa Sensation, 2010). This followed by the introduction of Christianity to the islands by John Williams and Charles Barf from the London Missionary Society, which resulted in the abandoning of the Samoan religions. Samoa became part of the trade lines, when a German funded merchants and shipping company Gedefroy and Sons, who were in control of the trading in South and Central Pacific in 1850's, has founded their depot at Apia (Godefroy and Company, 2010). German influence lead to the Berlin treaty in 1889. Samoa was guaranteed a political independence, but the king was under the American, British and German consul. This treaty was replaced by a German-American control in 1889. Germany took control of the Western Samoa was controlled by Germany, and Eastern Samoa was named American Samoa in the following years. Eastern Samoa has stayed as an American territory up to now; on the other hand, Western Samoa was invaded by New Zealand during the World War I (New Zealand History, 2010). Western Samoa became independent in 1962 and joined the Commonwealth in 1970.

Samoan Islands are located in the South Pacific, approximately half was between the New Zealand and Hawaiian Islands. American Samoa is 3000 km north of New Zealand, 4000 km North East of Australia and 4000 km South West of Hawaiian Islands, formed as a volcanic island chain located at the North East end of Tonga Trench. The American Samoa land area is only about 199 km^2, with a population of 66,432 people (CIA, 2010). Islands are exposed to intense typhoon season with an annual rainfall of 200 inch and American Samoa is a formation of five volcanic islands and two coral atolls (Colonial Voyage, 2010). Pago Pago has one of the best protected naturally protected deep harbor in the South Pacific and the tuna fishing and canneries is the primary source of income on the island that accounts for 80% of the employment. An aerial view of Pago Pago Harbor viewed from the Pacific Ocean is shown in Figure 3, and pictures of Pago Pago are

shown in Figure 4 (http://www.travelpod.com/s/photos/Pago+pago).

3.2 Historical events and water level data

American Samoa is only 200 km away from the Tonga trench, which was the distance from the epicenter of 2009 Samoan earthquake to the island of Tutuila. At Tonga trench Pacific plates subducts under the Australian plate at rate185 mm/yr (Stein and Okal, 2007), which is faster than any other plate convergence world wide (Kenji, 2010). The seismically active South Pacific region have experienced tsunamigenic earthquakes from Kermadec Islands (1986, 1976), Fiji (1937, 1919), Tonga (2009, 2006, 1919) and Vanuatu, as well as the 2009 Samoan Earthquake that triggered a tsunami which accounts for 189 fatality in the Samoan Islands, 34 of them from the American Samoa (Okal et. Al, 2010; Fritz et al, 2009). NOAA employee Gordon Yamasaki has provided real-time pictures from Pago Pago during the 2009 tsunami (Figure 5).

National Ocean Survey (NOS) tide gauge number 1770000 located at the Pago Pago Harbor at and was selected as the warning point for Pago Pago, American Samoa. Figures 3 and 4 shows the location of the tide gauge sensor inside the Pago Pago Bay at the North East corner of the Department of Marine and Wildlife Resources building shown in Figure 5e. The tide gauge has recordings of the 1952 Kamchatka, 1960 Chile, 1996 Andreanov, 2007 Chile, 2007 Peru, 2009 Samoa and 2010 Chile tsunamis that are used in the benchmarking of the reference and forecast model for Pago Pago for tide gauge comparison and inundation distances.

3.3 Model Setup

The high-resolution Pago Pago Harbor reference model consists of three nested grids. The outermost or A-grid covers most of Samoan Islands extending to a part of Tonga Trench with maximum depth of 8106 m with 12–arc-sec resolution. The intermediate, or B-grid, extends offshore of Tutuila to a depth of 3114 m with 1–arc-sec resolution. The innermost or C-grid encompasses only Pago Pago at a resolution of 1/3 arc-sec. Extents of the three nested grids are plotted on the Figure 2. This grid includes a steep bathymetric gradient with relief from a depth of 110 m up to a height of 624. Specific details of both reference and forecast model grids, including extents, are provided in Table 1.

The Pago Pago tsunami forecast model was optimized to decrease the computation time necessary for real-time forecasting of tsunami inundation during an event. A reference model simulation of three hours requires 13.3 hours of computation, whereas the optimized forecast model reduces the computation time of an 8 hours simulation to 8.8 minutes of wall-clock time. Relative computation times for both the reference and forecast models are provided in Table 1.

3.4 Propagation Database and Tsunami Sources

Worldwide ocean coastal zones have been partitioned into discrete fault segments of 100 km in length by 50 km in width for the purpose of modeling tsunamis generated from all possible source locations. Tsunami waveforms across each ocean basin over all grid points emanating from each discrete segment, or unit source, following a unit (1 m) slip earthquake have been pre-computed and are contained in a set of ocean-specific propagation databases (Gica *et al.,* 2008). The underlying assumption is that the deep–sea evolution is linear, even though the equations used for propagation are nonlinear. In deep water the contributions of the nonlinear terms in the wave evolution are negligible. Once in shallow water, the superposition probably is not applicable, hence a site–specific inundation model is created to study the terminal effects (Uslu, 2008).

The Pacific Basin propagation database, utilized for Samoa tsunami forecast model development, contains unit sources from the Aleutians/Alaska and Cascadia (AASZ), Central and South America (CSSZ), Eastern Philippines (EPSZ), Kuril Islands/Japan, and Mariana (KISZ), Manus (MOSZ), New Guinea (NGSZ), Ryuku-Nankai (RNSZ), New Zealand and Tonga (NTSZ), and New Britains and Vanuatu (NVSZ) source regions. Unit sources can be linearly combined to accommodate large seismic ruptures and can also be scaled to actual slips.

4.0 Results and Discussion

Tsunamis generated during the 1952 Kamchatka, the 1960 Chile, and the 1996 Andreanov, 2007 Chile, 2007 Kuril Islands, 2007 Peru, 2009 Samoa and 2010 Chile were measured at the Pago Pago tide gauge. A maximum wave height of approximately 2.5 m was observed during the 2009 Samoa Tsunami. Synthetic scenarios were used to test the stability of the Pago Pago tsunami forecast model and were compared to the reference model. Pago Pago tsunami forecast model predicts the historical records fairly well and the model will be part of the future NOAA tsunami forecast capabilities. Model is reliable not only for forecast, but also for future tsunami hazard assessment studies.

4.1 Model Validation

Historical tsunami observations recorded on marigraphs during the eight historical earthquakes recorded in the Pacific Ocean Basin were compared with model results for each event to validate the performance of the Pago Pago reference and forecast models. Historical events tested in this model cover three of the most active subduction zones with trans-oceanic tsunamis (ACSZ, KISZ and CSSZ) and an additional local tsunami triggered by the 2009 Samoa Earthquake. Specific information about each historical earthquake is provided in Table 2 and the epicenter of these events in Pacific Ocean are shown in Figures 6.Tide gauge comparisons between modeled time series and observed tsunami signal during each of the three earthquake case studies used for validation is provided in Figures 7-14. Overall, both the forecast and reference model predict the tide gauge observation fairly well. There is an arrival time offset in Figure 7 for 1952 Kamchatka model, however, the source for this event is not from an inversion that

includes tsunameter or tide gauge results, and the model predicts the amplitude and wave phase quite well. The models under-estimates the amplitude of the sixth wave from the 2007 Chile tsunami in Figure 10, which is approximately 5.75cm of the, however, the models do a good job from the tsunamis from Chile and Peru in 1960, 2007 and 2010 with higher amplitudes ranging from 10cm in 2007 Peruvian tsunami up to 1 m in 1960 Chilean tsunami in Figures 8, 12 and 14. The tide record from 1996 Andreanov in Figure 9 has a high noise level compared to the recorded 10 cm wave and there are two clipping in the record 2007 Kuril Islands tsunami in Figure 11. Figure 15 shows the post-tsunami survey results of 2009 Samoan earthquake and how they compared to the reference model. The survey and modeled results show that the Pago Pago harbor is more vulnerable at the west end of the harbor where the waves are focused the inundation distances where longer. Wave amplitude is well predicted by both the reference and forecast models with no anomalous behavior of either model when compared with one another.

4.2 Model robustness and Stability

The Pago Pago tsunami forecast model was tested for stability and robustness with a total of 19 mega, two medium and two micro synthetic scenarios listen in Table 3 using the Method of Splitting Tsunamis (MOST), Titov and Synolakis (1997, 1998). Tsunami sources were modeled by linearly combining NOAA propagation database unit sources to create these larger, seismic events. The underlying assumption is that the deep–sea evolution is linear, even though the equations used for propagation are nonlinear. Source information for each scenario is provided in Table 3 and the locations of each source are plotted in Figure 16. Since the forecast model will be used mostly for medium earthquakes size tsunamis, it is essential to test it with medium and micro tsunamis. The model performs well with two medium size tsunamis originated from Samoa and Japan, and three micro-tsunamis with amplitudes less than 10 cm originated from Western Aleutians and Southern Chile in Figures 17-39.

5.0 Summary and Conclusions

A set of reference inundation and optimized tsunami forecast grids have been developed for Pago Pago, American Samoa. The computational grids were derived from the best available bathymetric and topographic data at the time of grid construction. Eight historical events were simulated and forecast model results were compared with those of the high-resolution reference model to validate the performance of the forecast model. The stability and sensitivity of the model were tested with 24 different hypothetical scenarios. 18 of these are Mw 9.4, two of them Mw 8.0 and two of them were Mw 7.5 testing the stability of the model with smaller amplitude tsunamis. The forecast model remained stable during all historical event based validation testing and all synthetic scenario testing. The 18 Mw 9.4 scenarios test Pago Pago for worst-case scenarios from the Pacific Rim. A 4 m waves is expected from Western Aleutians (Figure 17), 2 m wave from Cascadia (Figure 21), 7 m wave from Southern Chile (Figure 25), 7 m from Kamchatka (Figure 27), 4.5 m from Vanuatu (Figure 34) and a wave larger than 15 m from a local tsunami on Tonga trench (Figure 33). Forecast model and reference model agree with each other for the initial three waves for all events, however, the reference model captures the later waves and the resonance in the harbor much better. Even though the forecast model is satisfactory fore prediction in real-time, a more detailed hazard assessment study requires higher resolution.

The 2009 Mw 8.1 Samoa earthquake caused substantial damage to the US territories and neighbors and 189 fatalities. South Pacific distant from the Kurils Islands, Aleutians, Alaska or South American Subduction zones, and volcanic formation of the islands may help dissipate some of the danger. However, the islands are neighbor to the Tonga trench that has highest strain accumulation world wide (Stein and Okal, 2007; Kenji, 2010). Since, the islands are exposed to frequent natural disasters from earthquakes and typhoons, the NOAA's tsunami forecast model will be essential part of the hazard mitigation.

6.0 Acknowledgments

The authors wish to thank the NOAA Center for Tsunami Research group for discussions, comments, and editorial assistance and Ryan Layne Whitney for technical assistance and editorial review of this report. Collaborative contributions of the National Weather Service, the National Geophysical Data Center, and the National Data Buoy Center were invaluable.

The National Oceanic and Atmospheric Administration provided funding for all work culminating in the development of the Apra Harbor, Guam tsunami forecast model and report. This publication was partially funded by the Joint Institute for the Study of the Atmosphere and Ocean (JISAO) under NOAA Cooperative Agreement No. NA17RJ1232, JISAO Contribution No. 1829. This is PMEL Contribution No. 3373.

7.0 References

CIA (2010):The World Factbook. https://www.cia.gov/library/ publications/the-world-factbook/index.html.

Colonial Voyage (2010). American Samoa http://www.colonialvoyage.com/viaggi/asamoa.html

Fritz, H. M.; Borrero, J. C.; Okal, E.; Synolakis, C.; Weiss, R.; Jaffe, B. E.; Lynett, P. J.; Titov, V. V.; Foteinis, S.; Chan, I.; Liu, P. (2009). Reconnaissance Survey of the 29 September 2009 Tsunami on Tutuila Island, American Samoa, Eos Trans. AGU, 90(52), Fall Meet. Suppl., Abstract U23F-04.

Godefroy and Company (2010). Godefroy & Company, Hamburg Merchants & Shippers, http://homepages.ihug.co.nz/~tonyf/godeffroy/godeffroy.html

Gica, E., Spillane, M., Titov, V., Chamberlin, C., and Newman, J. (2008). Development of the forecast propagation database for NOAA's Short–term Inundation Forecast for Tsunamis (SIFT). Tech. Memo. OAR PMEL–139 NTIS: PBB2008- 109391, NOAA/Pacific Marine Environmental Laboratory, Seattle, WA.

Kenji, S. (2010). Earthquakes: Double trouble at Tonga. Nature, 466 , 931–932, doi:10.1038/466931a.

New Zealand History (2010). New Zealand goes to war http://www.nzhistory.net.nz/war/new-zealand-goes-to-war-first-world-war

Okal, E. A., Hermann M. Fritz, Costas E. Synolakis, Jose C. Borrero, Robert Weiss, Patrick J. Lynett, Vasily V. Titov, Spyros Foteinis, Bruce E. Jaffe, Philip L. F. Liu, and I-chi Chan. (2010). Field survey of the Samoa tsunami of 29 September 2009 Seismological Research, 81(4):577-591

Samoa Sensation (2010). Samoan Sensation http://www.samoa.co.uk/history.html

Stein, S. and Okal, E. A. (2007). Ultralong period seismic study of the December 2004 Indian Ocean earthquake and implications for regional tectonics and the subduc- tion process. Bulletin of the Seismological Society of America, 97:S279–S295.

Synolakis, C.E., E.N. Bernard, V.V. Titov, U. Kânoğlu, and F.I. González (2008): Validation and verification of tsunami numerical models. Pure Appl. Geo- phys., 165(11–12), 2197–2228.

Tang, L., C. Chamberlin, E. Tolkova, M. Spillane, V.V. Titov, E.N. Bernard, and H.O. Mofjeld (2006): Assessment of potential tsunami impact for Pearl Harbor, Hawaii. NOAA Tech. Memo. OAR PMEL-131, NTIS: PB2007-100617, 36 pp.

Tang, L., V.V. Titov, Y. Wei, H.O. Mofjeld, M. Spillane, D. Arcas, E.N. Bernard, C. Chamberlin, E. Gica, and J. Newman (2008): Tsunami forecast analysis for the May 2006 Tonga tsunami. J. Geophys. Res., 113, C12015, doi: 10.1029/2008JC004922.

Tang, L., V.V. Titov, and C.D. Chamberlin (2009): Development, testing, and applications of site-specific tsunami inundation models for real-time forecasting. J. Geophys. Res., 114, C12025, doi: 10.1029/2009JC005476.

Titov, V. V. and González, F. (1997). Implementation and testing of the method of splitting tsunami (MOST) model. Technical Memorandum ERL PMEL 112, NOAA.

Titov, V. V. and Synolakis, C. E. (1997). Extreme inundation flows during the Hokkaido-Nansei-Oki tsunami. Geophys. Res. Lett., 24(11):1315–1318.

Titov, V. V. and Synolakis, C. E. (1998). Numerical modelling of tidal wave runup. J. Waterw. Port Coast. Ocean Eng., 124:157–171.

Titov, V. V., González, F. I., Bernard, E. N., Eble, M. C., Mofjeld, H. O., Newman, J. C., and Venturato, A. J. (2005). Real-time tsunami forecasting: Challenges and solutions. Natural Hazards, 35(1):35–41.

Titov, V.V. (2009): Tsunami forecasting. Chapter 12 in The Sea, Volume 15: Tsunamis, Harvard University Press, Cambridge, MA and London, England, 371–400.

Wei, Y., E. Bernard, L. Tang, R. Weiss, V. Titov, C. Moore, M. Spillane, M. Hopkins, and U. Kânoğlu (2008): Real-time experimental forecast of the Peruvian tsunami of August 2007 for U.S. coastlines. Geophys. Res. Lett., 35, L04609, doi: 10.1029/2007GL032250.

Uslu, B. (2008). Deterministic and Probabilistic tsunami studies in California from near and farfield sources. PhD thesis, University of Southern California, Los Angeles, California.

Table 1: MOST setup parameters for reference and forecast models for Pago Pago, American Samoa.

		Reference Model				Forecast Model			
Grid	Region	Coverage Lat. [ºS] Lon. [ºW]	Cell Size [“]	nx x ny	Time Step [sec]	Coverage Lat. [ºS] Lon. [ºW]	Cell Size [“]	nx x ny	Time Step [sec]
A	South Pacific	15.80-13.20 and 169.30-13.00.	12	1110x781	1.2	15.76-14.10 and 171.60-170.07.	36	154x167	3.0
B	Tutuila	14.4-14.23 and 170.54-170.85.	1	1121x631	0.15	14.55-14.12 and 170.30-171.05.	15	181x104	1.5
C	Pago Pago	14.3-14.27 and 170.62-170.71.	1/3	995x411	0.15	14.30-14.26 and 170.65-170.71.	3s x 2s	76x69	1.5
Minimum offshore depth [m]				0.0001				0.001	
Water depth for dry land [m]				0.1				0.1	
Friction coefficient [n^2]				0.001				0.001	
CPU time for 8hr simulation				35.4 hours				8.8 minutes	

Computations were performed on a single Intel Xeon processor at 3.6 GHz, Dell PowerEdge 1850.

Earthquake / Seismic				Model		
Event	USGS Date Time (UTC) Epicenter	CMT Date Time (UTC) Centroid	Magnitude Mw	Tsunami Magnitude[1]	Subduction Zone	Tsunami Source
1946 Unimak	01 Apr 12:28:56 52.75ºN 163.50ºW	01 Apr 12:28:56 53.32ºN 163.19ºW	[2]8.5	8.5	Aleutian-Alaska-Cascadia (ACSZ)	7.5 × b23 + 19.7 × b24 + 3.7 × b25
1952 Kamchatka	04 Nov 16:58:26.0 [3]52.76ºN 160.06ºE	04 Nov 16:58:26.0 52.75ºN 159.50ºE	[3]9.0	8.7	Kamchatka-Kuril-Japan-Izu-Mariana-Yap (KISZ)	_
1960 Chile	22 May 19:11:14 [3]38.29ºS 73.05ºW	22 May 19:11:14 38.50ºS 74.50ºW	[4]9.5		Central-South America (CSSZ)	Kanamori and Ciper (1974)
1996 Andreanov	10 Jun 04:03:35 51.56ºN 175.39ºW	10 Jun 04:04:03.4 51.10ºN 177.410ºW	[5]7.9	7.8	Aleutian-Alaska-Cascadia (ACSZ)	2.40 × a15 + 0.80 × b16
2007 Kuril	13 Jan 04:23:20 46.272ºN 154.455ºE	13 Jan 04:23:48.1 46.17ºN 154.80ºE	[5]8.1	7.9	Kamchatka-Kuril-Japan-Izu-Mariana-Yap (KISZ)	-3.64 × b13
2007 Chile	14 Nov 15:40:50 22.204ºS 69.869ºW	14 Nov 15:41:11.2 22.64ºS 70.62ºW	[3]7.7	7.6	Central-South America (CSSZ)	z73 × 1.65
2009 Samoa	29 Sep 17:48:10 15.509ºS 172.034ºW	29 Sep 17:48:26.8 15.13ºS 171.97ºW	[5]8.1	8.1	New Zealand-Kermadec-Tonga (NTSZ)	[6]3.96 × a34 + 3.96 × b34
2010 Chile	27 Feb 06:34:14 35.909ºS 72.733ºW	27 Feb 06:35:15.4 35.95ºS 73.15ºW	[5]8.8	8.8	Central-South America (CSSZ)	[6]a88 × 17.24 + a90 × 8.82 + b88 × 11.86 + b89 × 18.39 + b90 × 16.75 + z88 × 20.78 + z90 × 7.06

[1] Preliminary source – derived from source and deep-ocean observations
[2] López and Okal (2006)
[3] United States Geological Survey (USGS)
[4] Kanamori and Ciper (1974)
[5] Centroid Moment Tensor
[6] Tsunami source was obtained in real time and applied to the forecast

Synthetic tsunami events

Scenario Name	Source Zone	Tsunami Source	α [m]
	Mega-tsunami Scenario		
ACSZ 6-15	Aleutian-Alaska-Cascadia	A6-A15, B6-B15	30
ACSZ 16-25	Aleutian-Alaska-Cascadia	A16-A25, B16-B25	30
ACSZ 22-31	Aleutian-Alaska-Cascadia	A22-A31, B22-B31	30
ACSZ 50-59	Aleutian-Alaska-Cascadia	A50-A59, B50-B59	30
ACSZ 56-65	Aleutian-Alaska-Cascadia	A56-A65, B56-B65	30
CSSZ 1-10	Central and South America	A1-A10, B1-B10	30
CSSZ 37-46	Central and South America	A37-A46, B37-B46	30
CSSZ 89-98	Central and South America	A89-B98, B89-B98	30
CSSZ 102-111	Central and South America	A102-A111, B102-	30
EPSZ 6-15	East Philippines	A6-A15, B6-B15	30
KISZ 1-10	Kamchatka-Yap-Mariana-Izu-	A1-A10, B1-B10	30
KISZ 22-31	Kamchatka-Yap-Mariana-Izu-	A22-A31, B22-B31	30
KISZ 32-41	Kamchatka-Yap-Mariana-Izu-	A32-A41, B32-B41	30
KISZ 56-65	Kamchatka-Yap-Mariana-Izu-	A56-A65, B56-B65	30
MOSZ 1-10	Manus-OCB	A1-A10, B1-B10	30
NGSZ 3-12	North New Guinea	A3-A12, B3-B12	30
NTSZ 30-39	New Zealand-Kermadec-Tonga	A30-A39, B30-B39	30
NVSZ 28-37	New Britain-Solomons-Vanuatu	A28-A37, B28-B37	30
RNSZ 12-21	Ryukus-Kyushu-Nankai	A12-A21, B12-B21	30
	Mw 7.5 Scenario		
NTSZ B36	New Zealand-Kermadec-Tonga	B36	1
RNSZ B14-15	Ryukus-Kyushu-Nankai	B14-B15	3
	Micro-tsunami Scenario		
ACSZ B6	Aleutian-Alaska-Cascadia	B6	0.01
CSSZ B115	Central and South America	B115	1

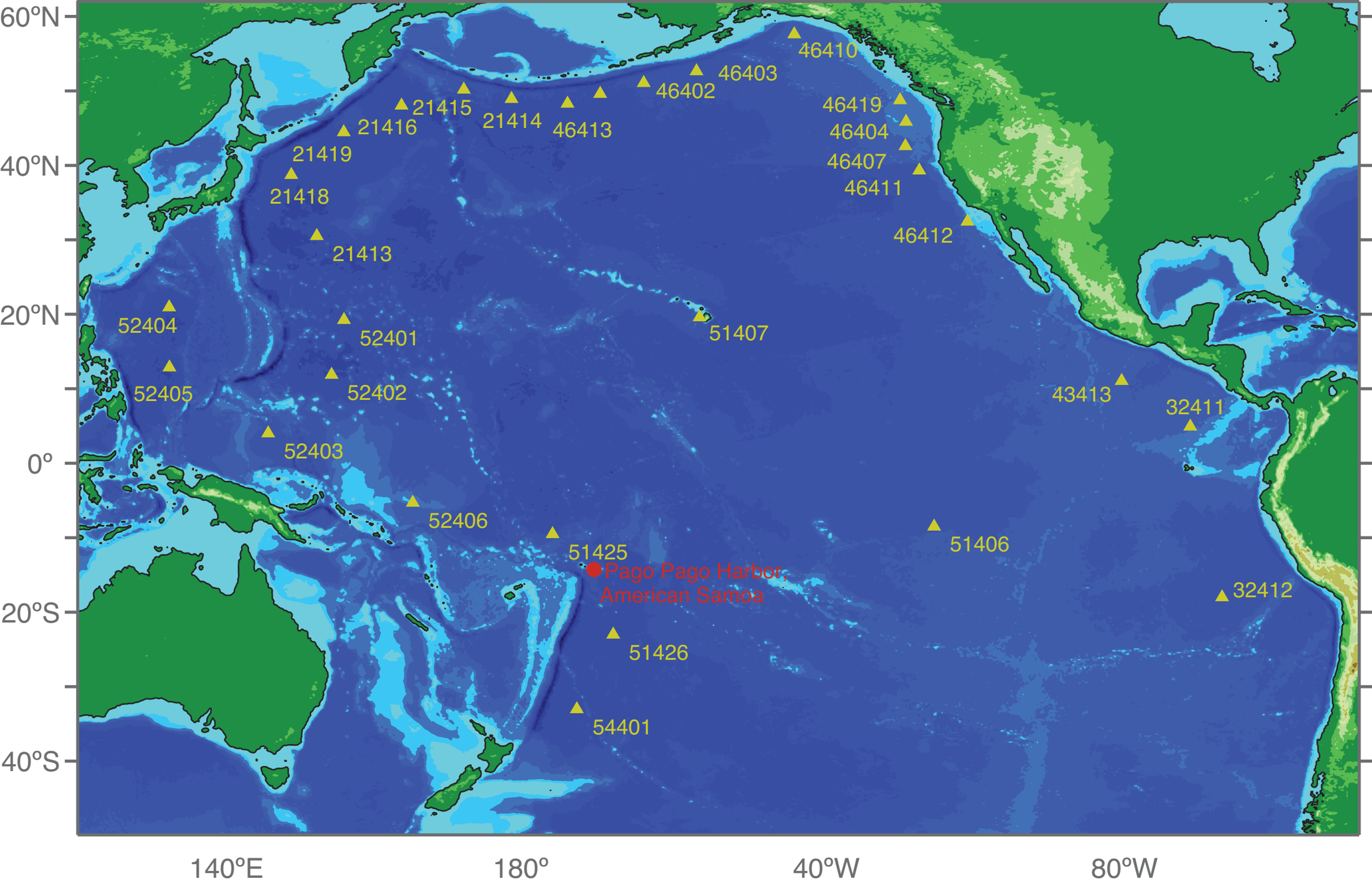
60°N
40°N
20°N
0°
20°S
40°S
140°E
180°
40°W
80°W
46410
46403
46402
21415
21414
46413
21416
46419
46404
21419
46407
21418
46411
46412
21413
52404
52401
51407
52405
52402
43413
32411
52403
52406
51425
Pago Pago Harbor,
American Samoa
51406
32412
51426
54401

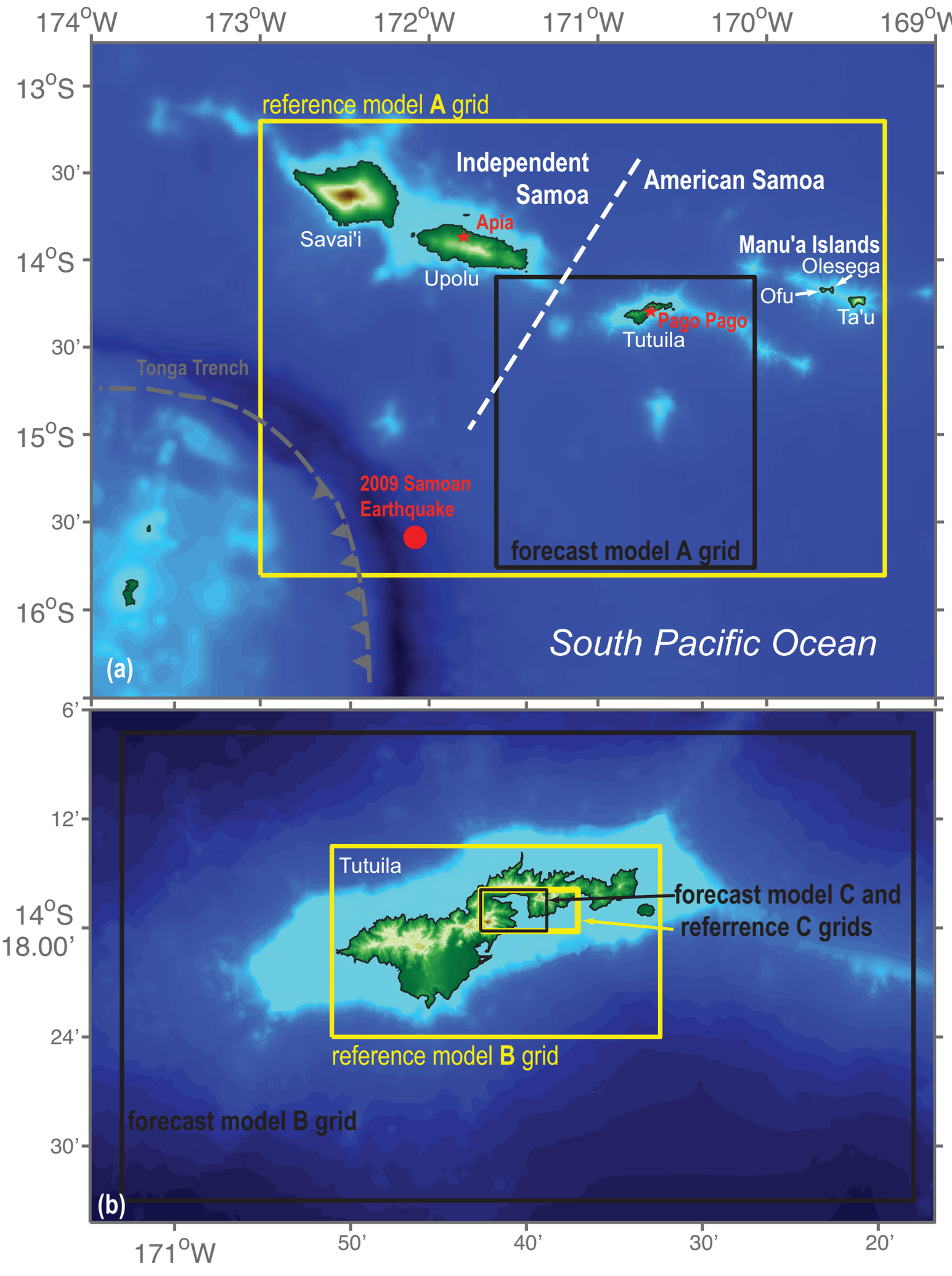
174°W
173°W
172°W
171°W
170°W
169°W
13°S
30'
14°S
30'
15°S
30'
16°S
reference model A grid
Independent Samoa
American Samoa
Savai'i
Apia
Upolu
Manu'a Islands
Olesega
Ofu
Ta'u
Pago Pago
Tutuila
Tonga Trench
2009 Samoan Earthquake
forecast model A grid
South Pacific Ocean
(a)
6'
12'
14°S
18.00'
24'
30'
Tutuila
forecast model C and
referrence C grids
reference model B grid
forecast model B grid
(b)
171°W
50'
40'
30'
20'

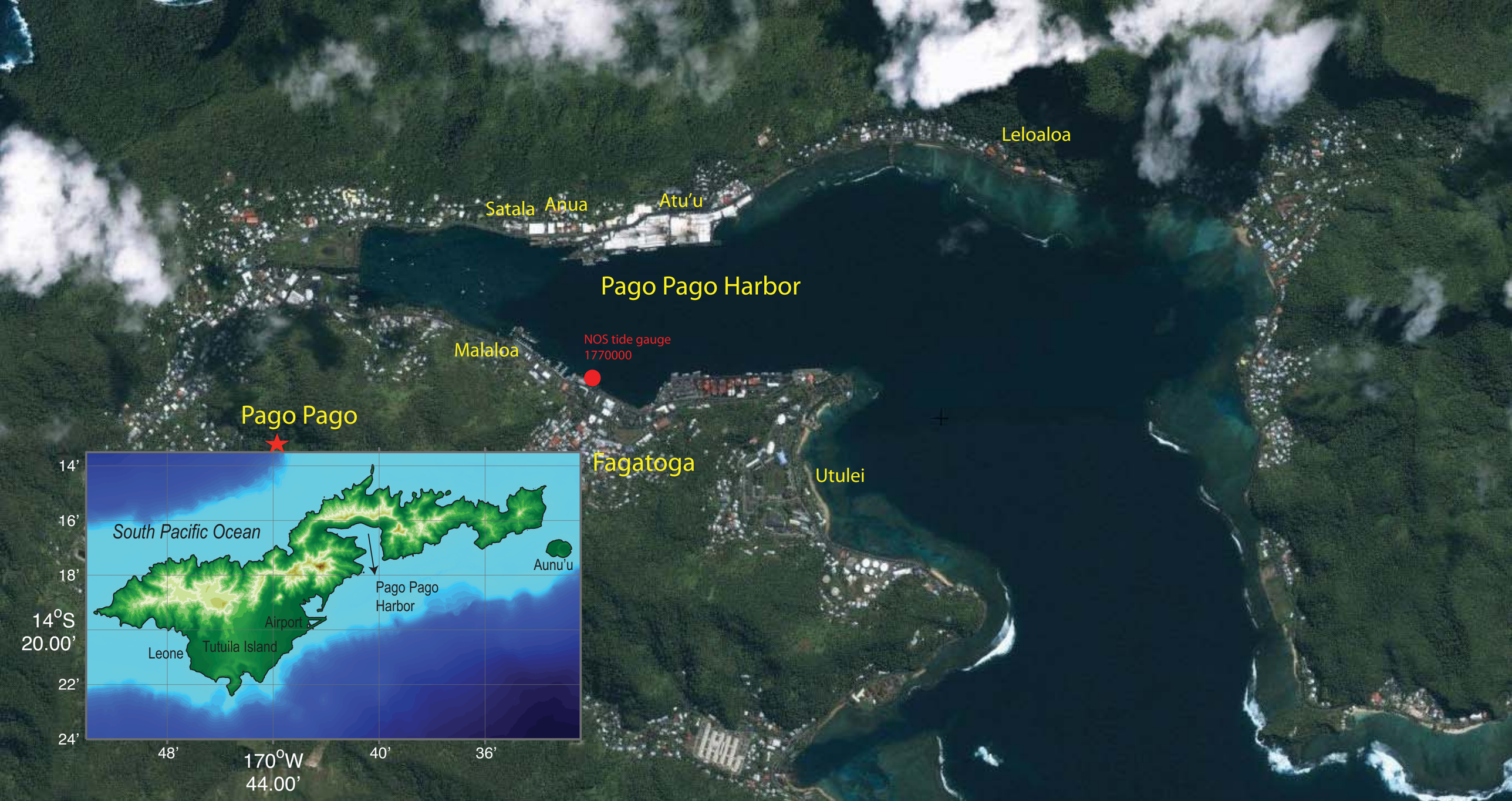
Leloaloa
Satala
Anua
Atu'u
Pago Pago Harbor
NOS tide gauge
1770000
Malaloa
Pago Pago
Fagatoga
Utulei
14'
16'
18'
14°S
20.00'
22'
24'
South Pacific Ocean
Aunu'u
Pago Pago
Harbor
Airport
Leone
Tutuila Island
48'
170°W
44.00'
40'
36'

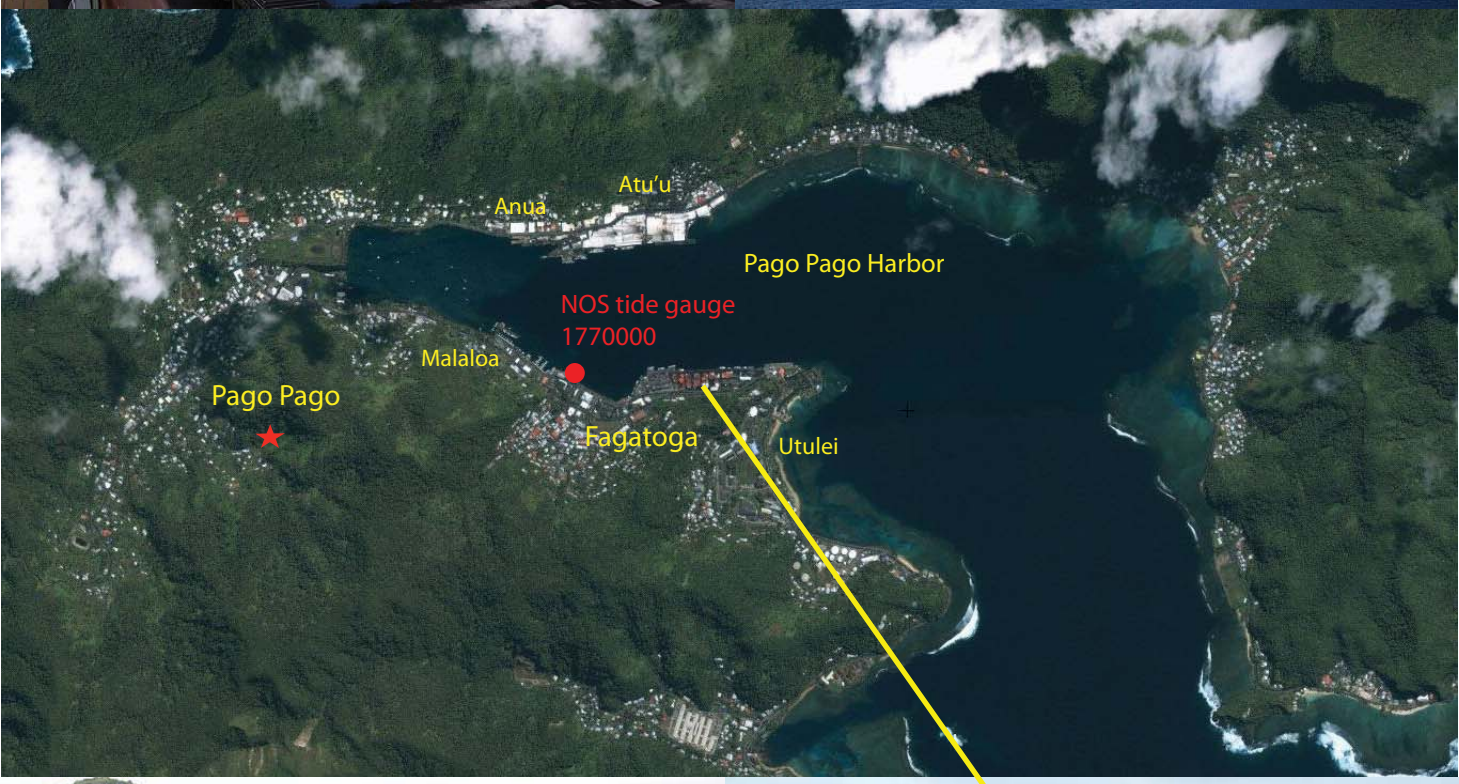
Anua
Atu'u
Pago Pago Harbor
NOS tide gauge
1770000
Malaloa
Pago Pago
Fagatoga
Utulei


a


b


d


c


e

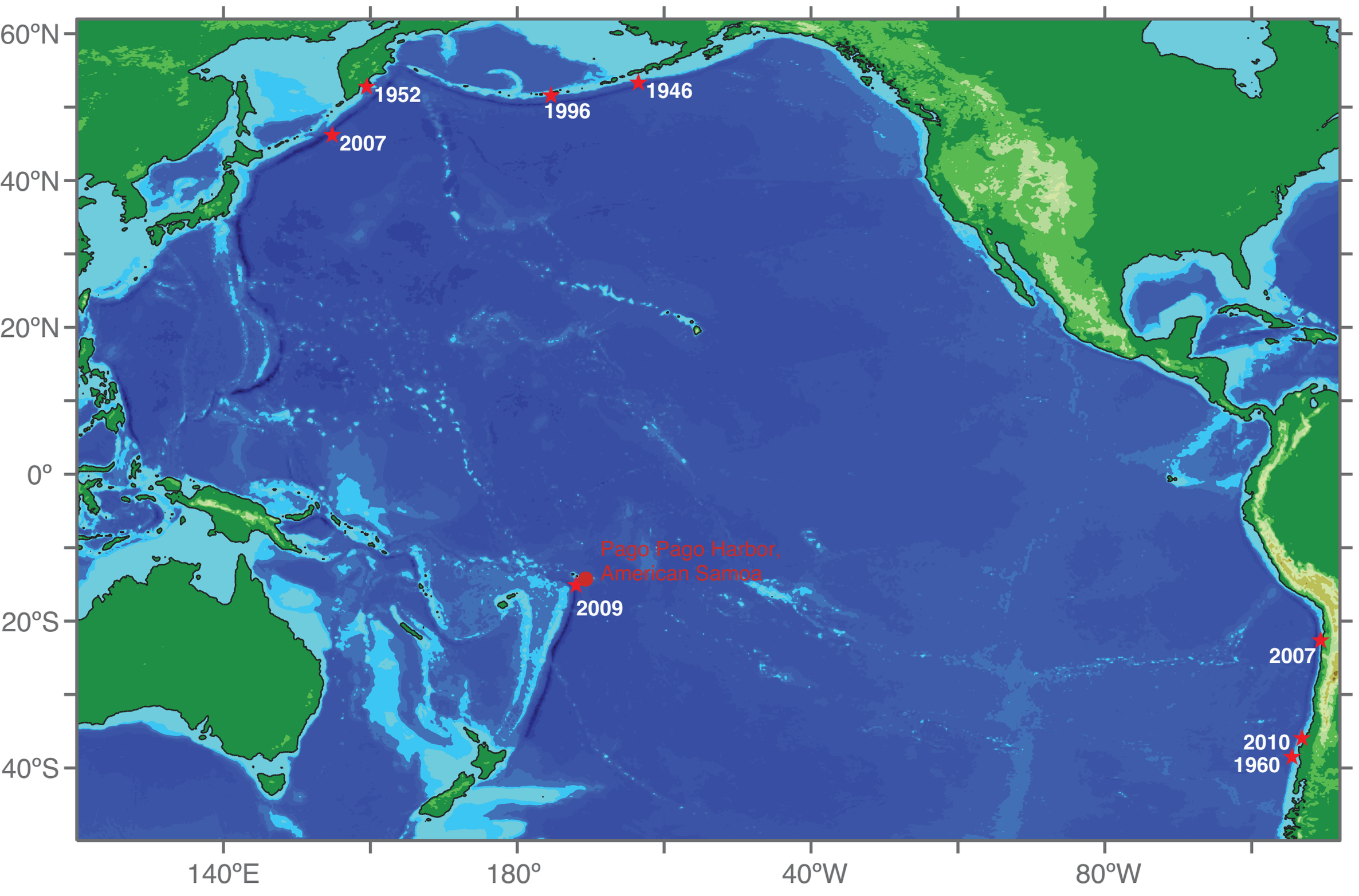
60°N
40°N
20°N
0°
20°S
40°S
140°E
180°
40°W
80°W
1952
1996
1946
2007
Pago Pago Harbor,
American Samoa
2009
2007
2010
1960

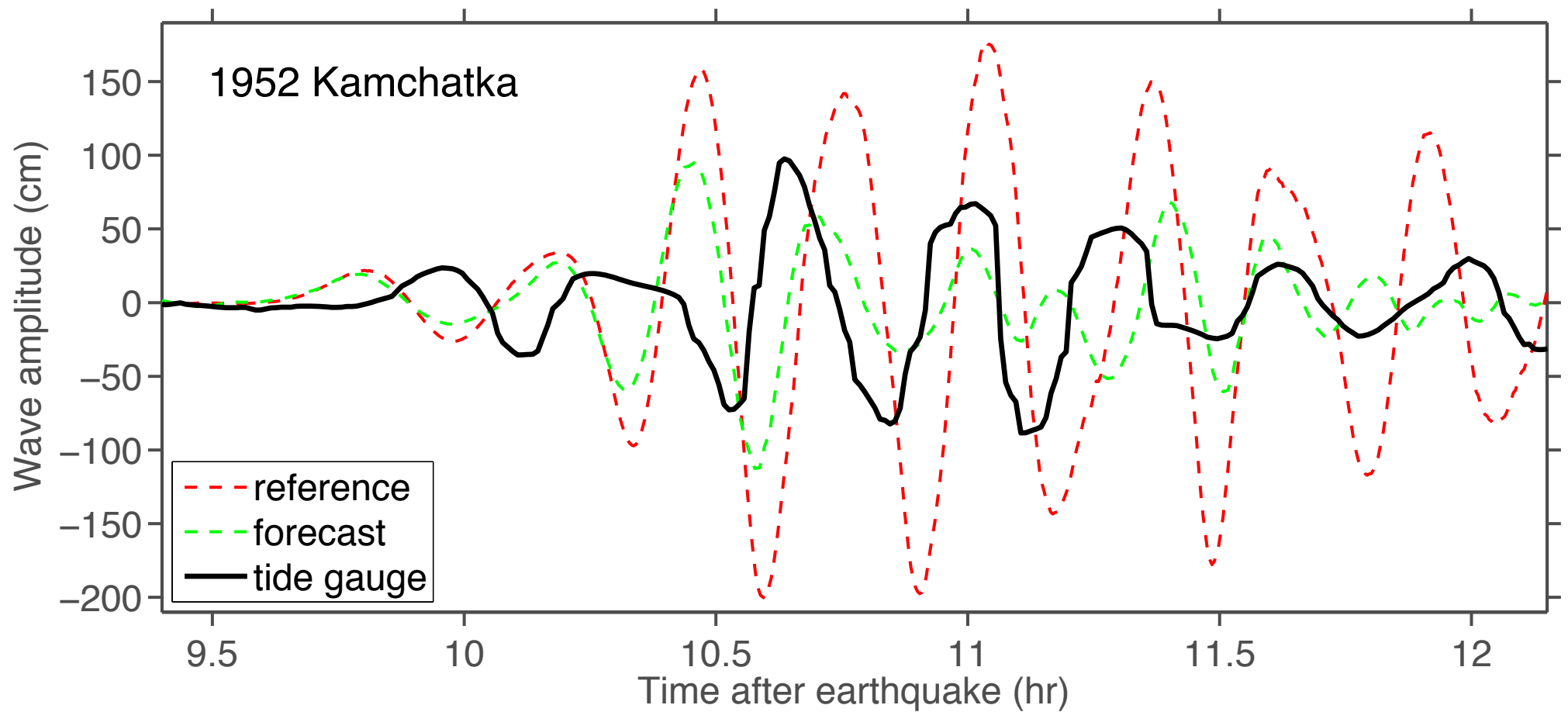
1952 Kamchatka
Wave amplitude (cm)
150
100
50
0
−50
−100
−150
−200
9.5
10
10.5
11
11.5
12
Time after earthquake (hr)
reference
forecast
tide gauge

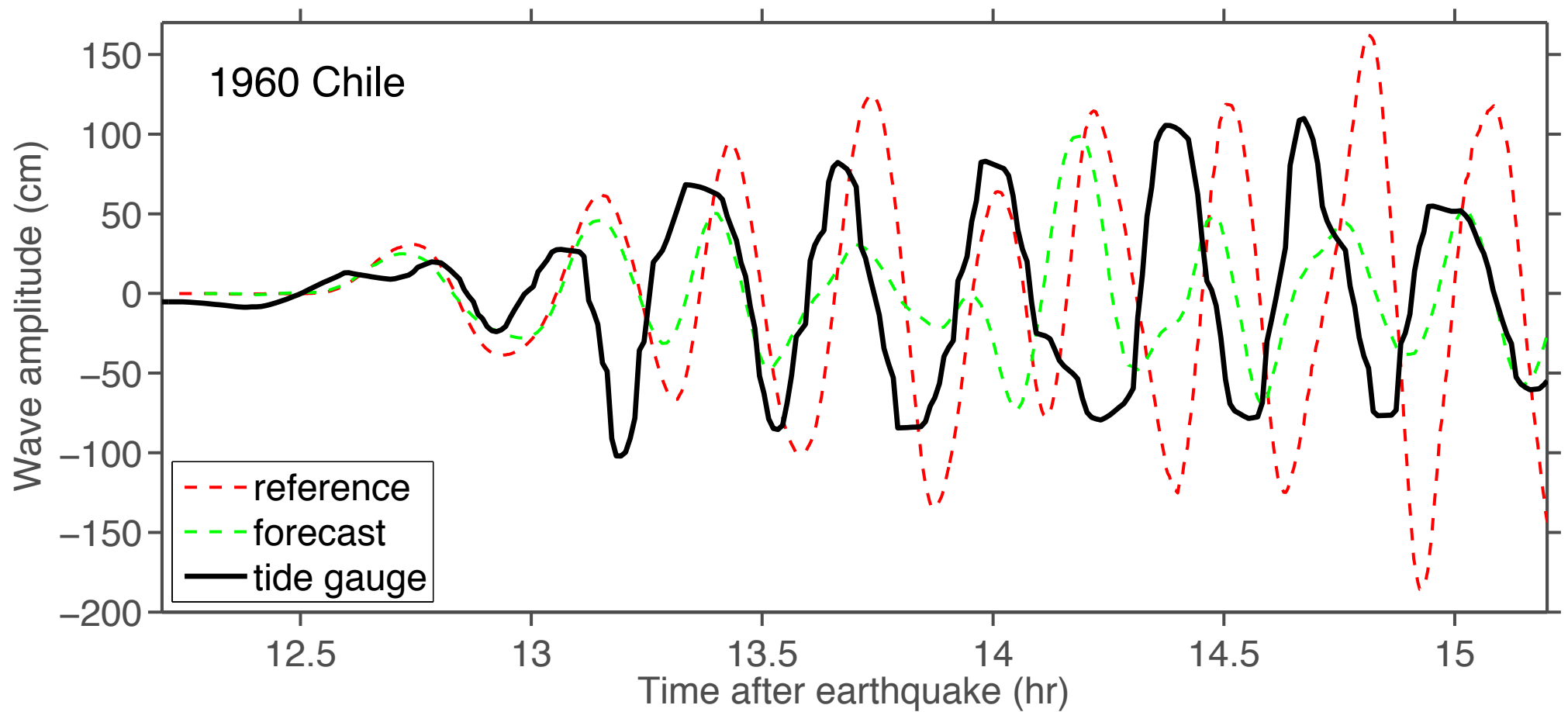
1960 Chile
Wave amplitude (cm)
150
100
50
0
−50
−100
−150
−200
12.5
13
13.5
14
14.5
15
Time after earthquake (hr)
reference
forecast
tide gauge

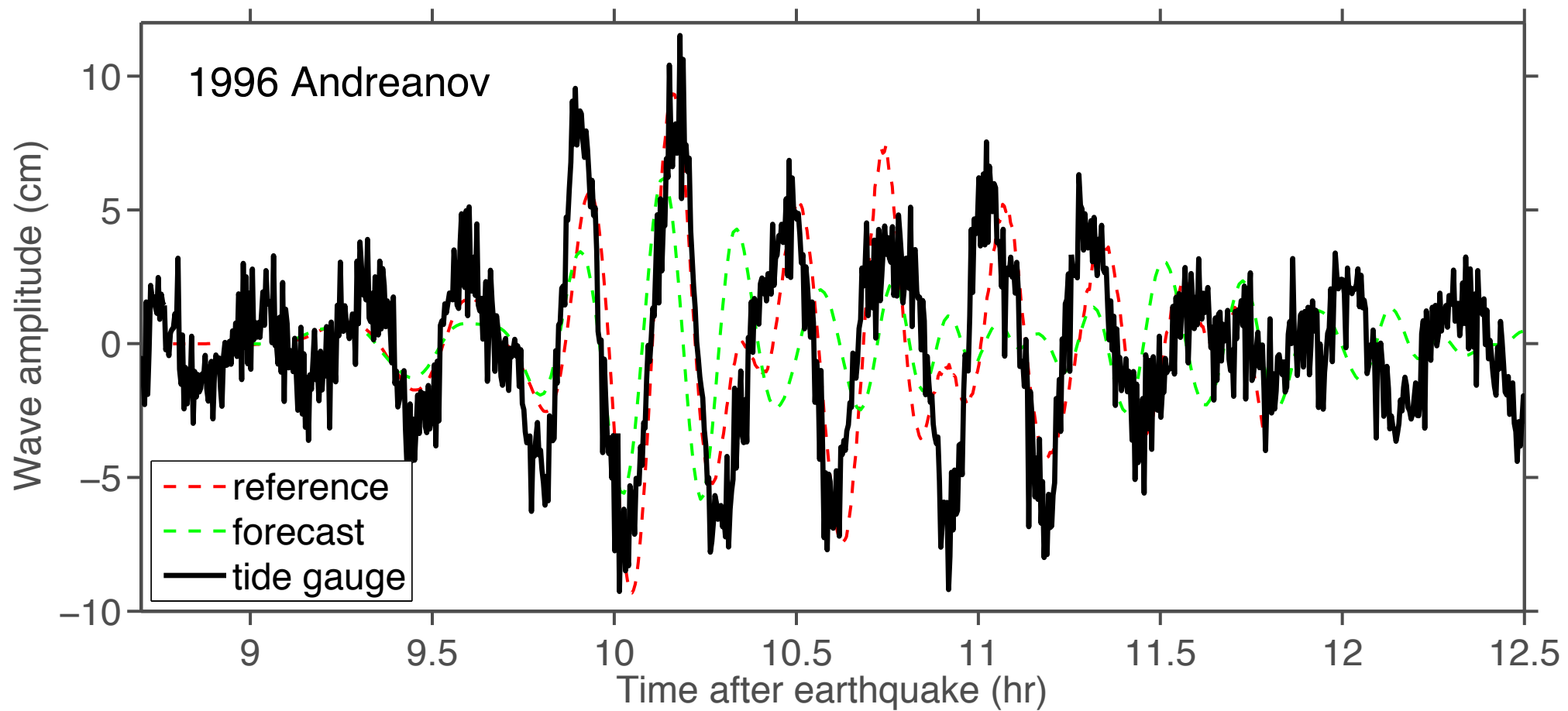
1996 Andreanov
reference
forecast
tide gauge
Wave amplitude (cm)
Time after earthquake (hr)
10
5
0
−5
−10
9
9.5
10
10.5
11
11.5
12
12.5

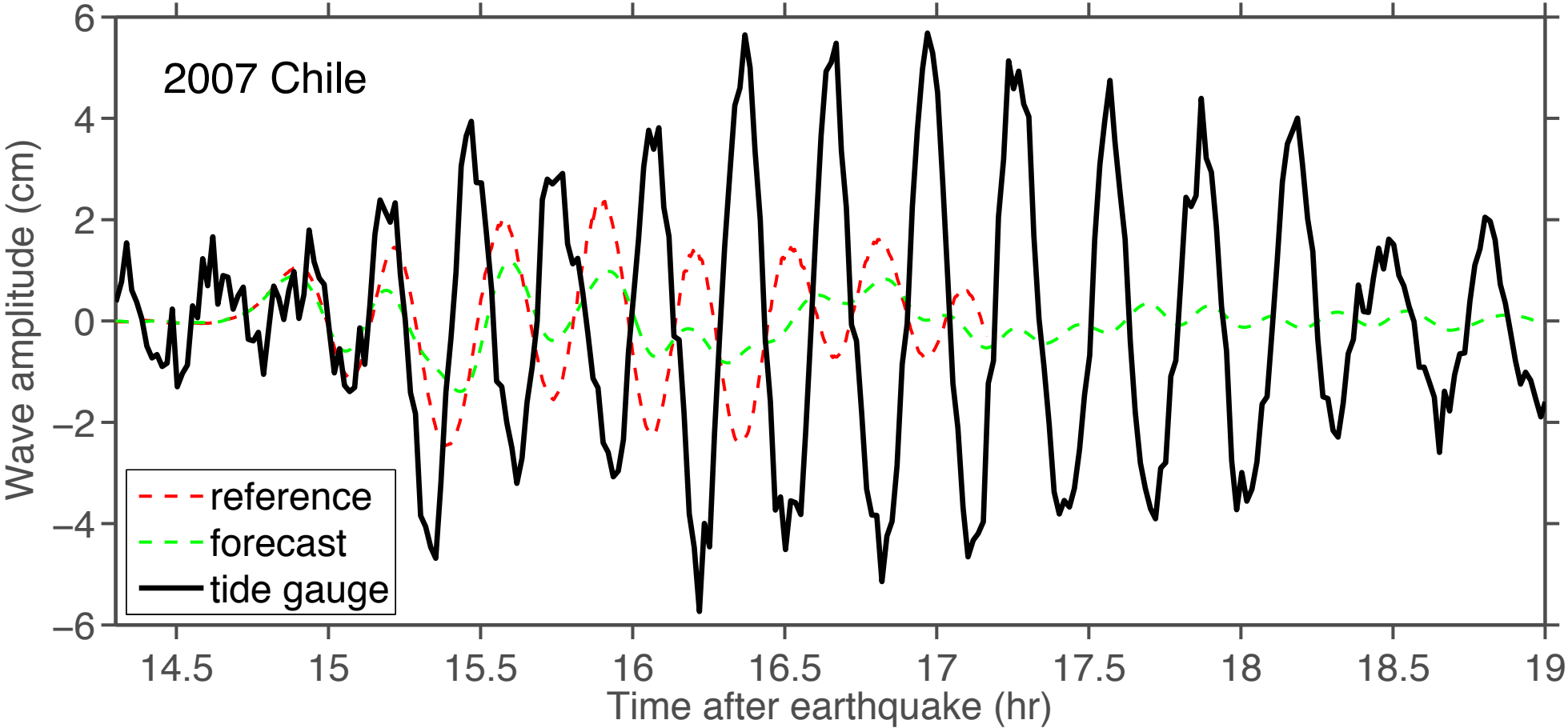
2007 Chile
reference
forecast
tide gauge
Wave amplitude (cm)
Time after earthquake (hr)
6
4
2
0
−2
−4
−6
14.5
15
15.5
16
16.5
17
17.5
18
18.5
19

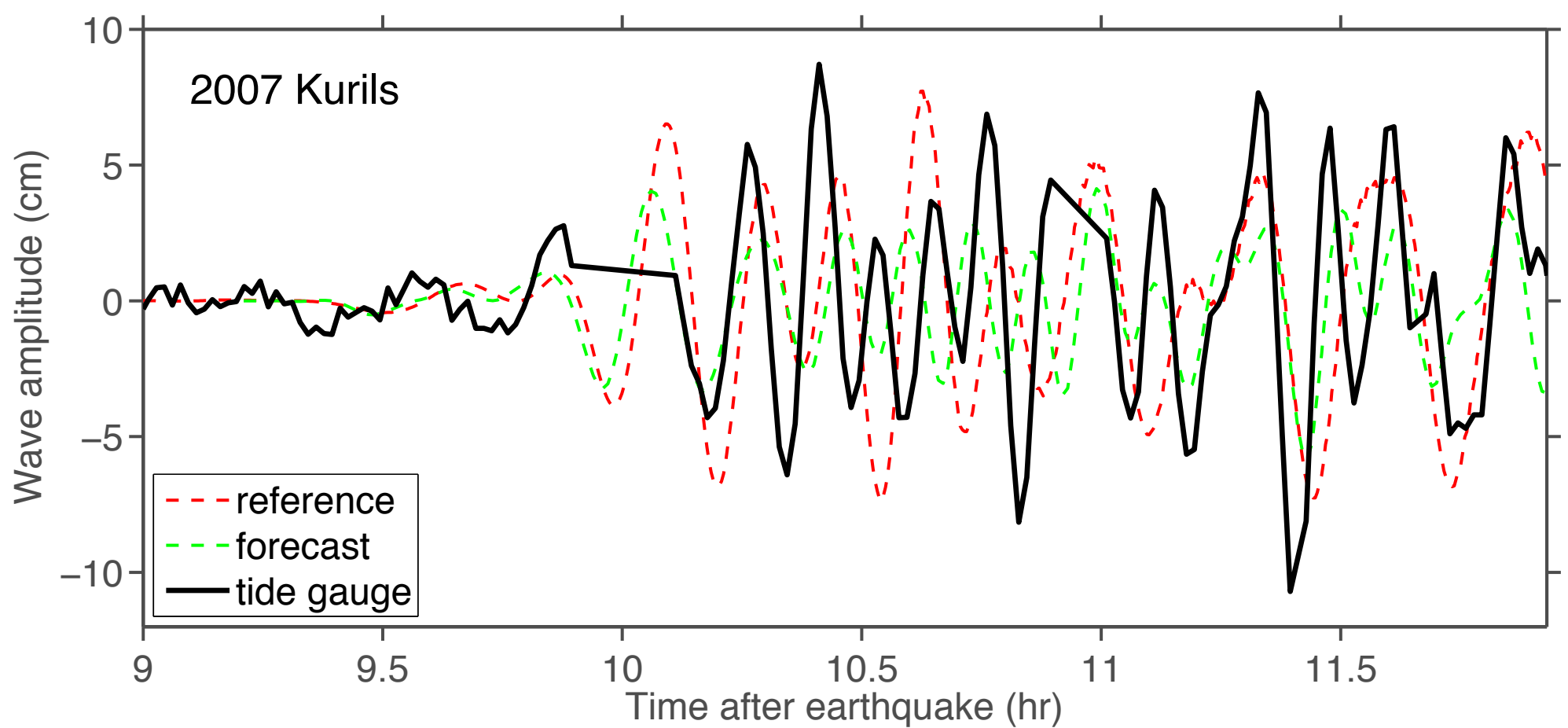
2007 Kurils
Wave amplitude (cm)
10
5
0
−5
−10
9
9.5
10
10.5
11
11.5
Time after earthquake (hr)
reference
forecast
tide gauge

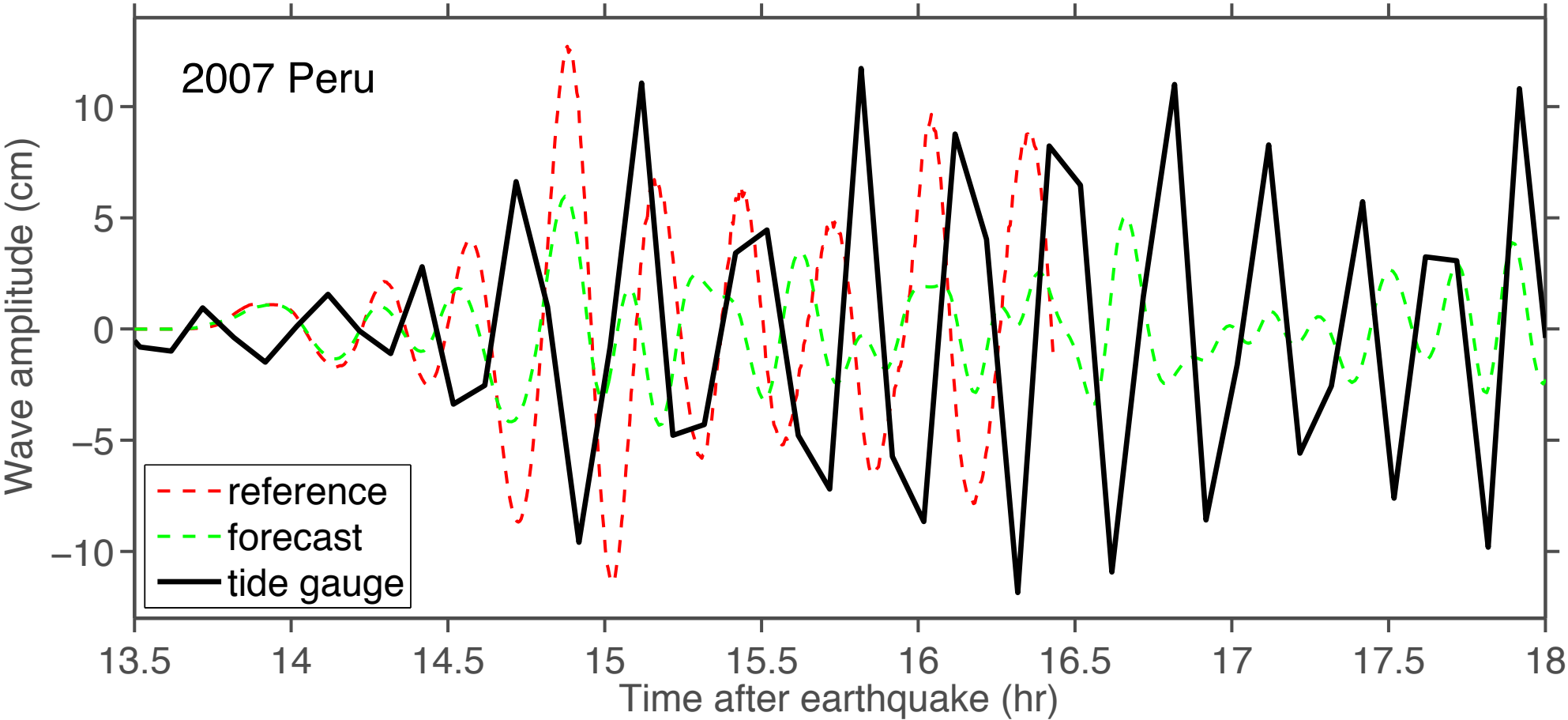
2007 Peru
Wave amplitude (cm)
10
5
0
−5
−10
reference
forecast
tide gauge
13.5
14
14.5
15
15.5
16
16.5
17
17.5
18
Time after earthquake (hr)

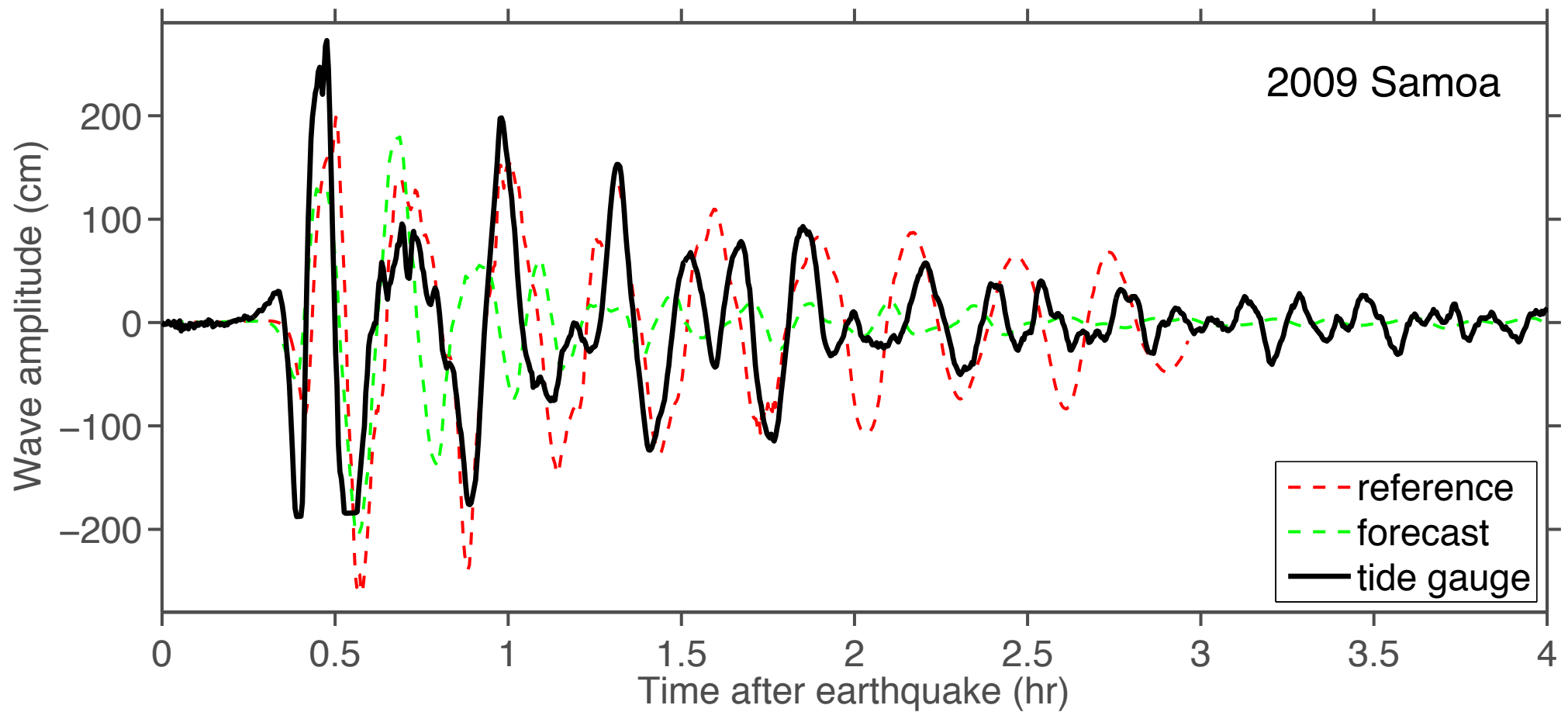
2009 Samoa
Wave amplitude (cm)
200
100
0
−100
−200
0
0.5
1
1.5
2
2.5
3
3.5
4
Time after earthquake (hr)
reference
forecast
tide gauge

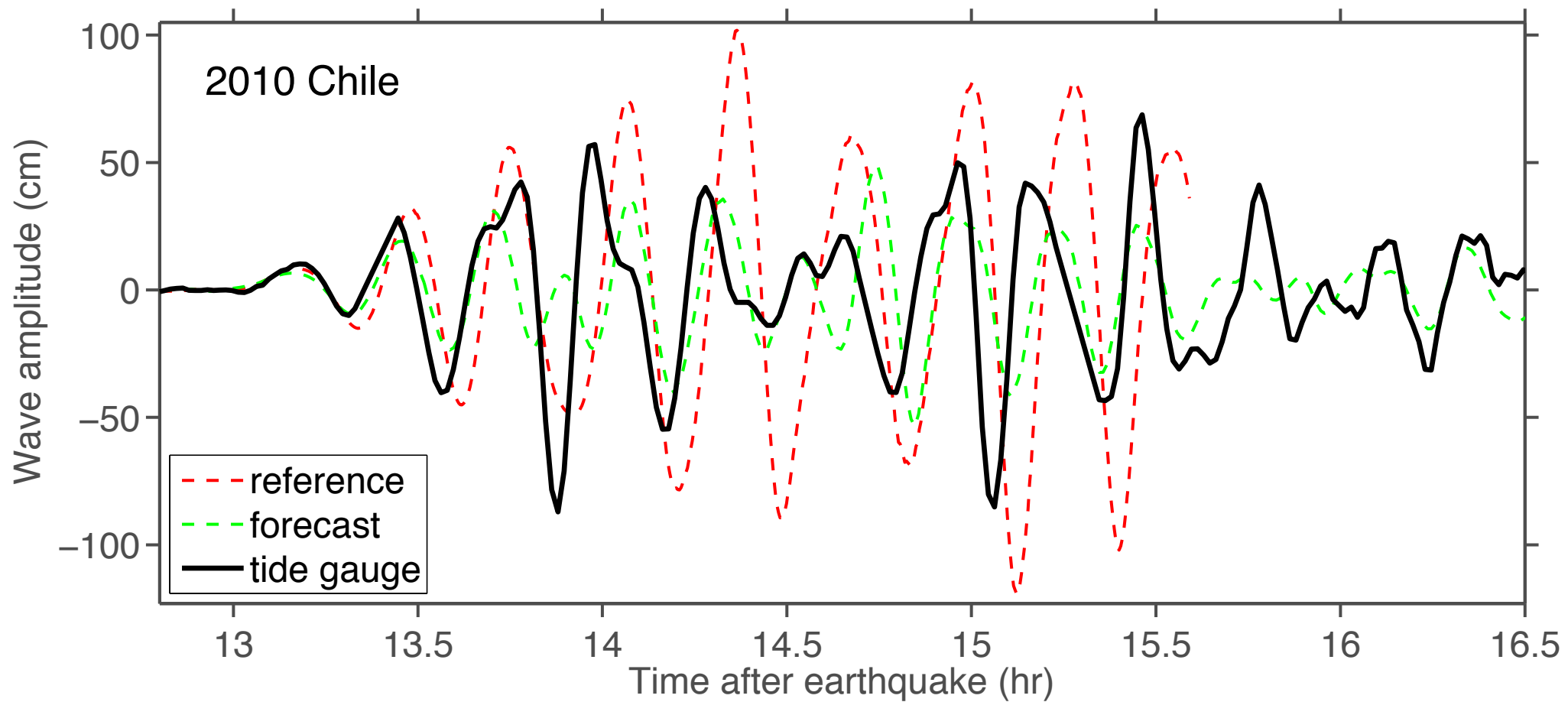
2010 Chile
reference
forecast
tide gauge
Wave amplitude (cm)
100
50
0
−50
−100
13
13.5
14
14.5
15
15.5
16
16.5
Time after earthquake (hr)

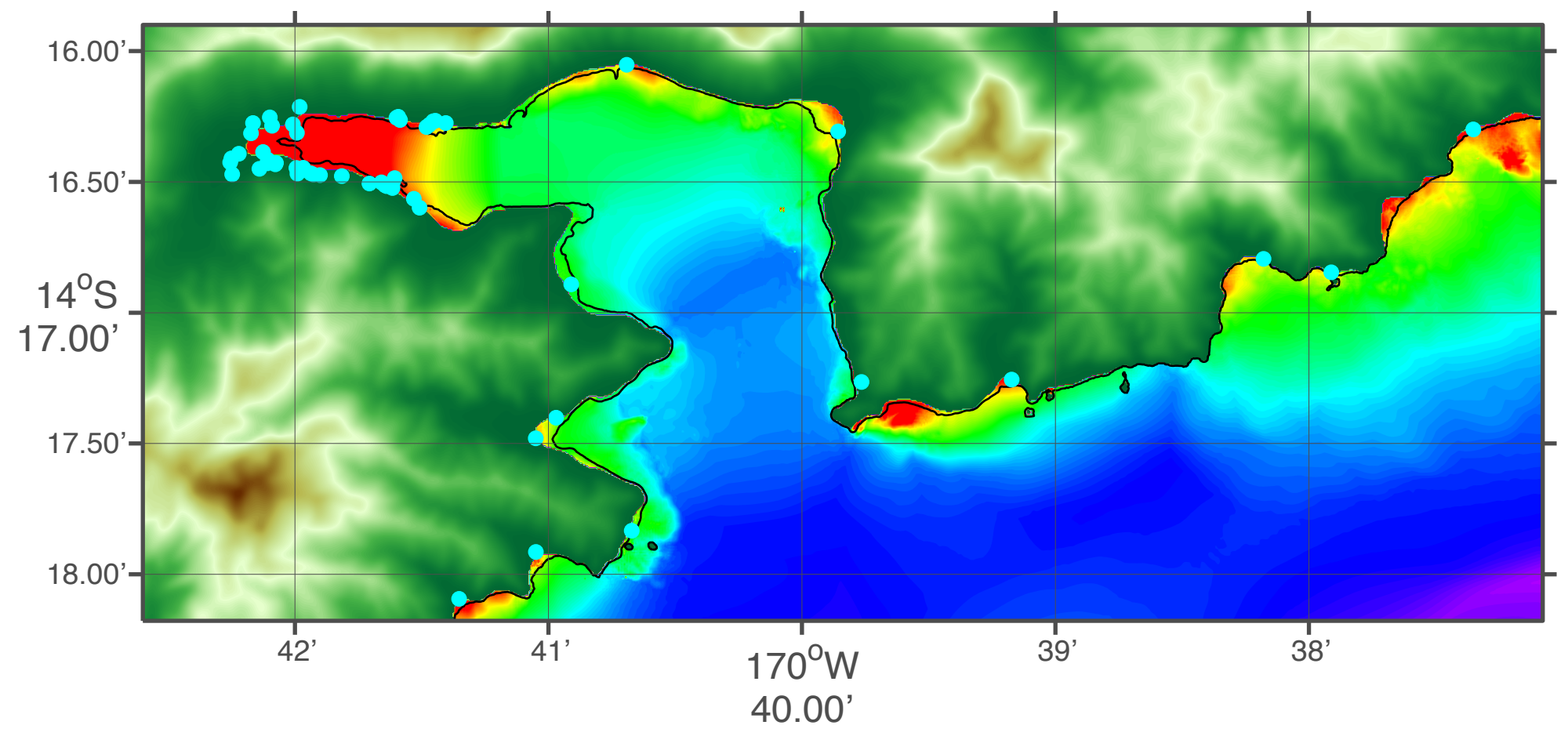
16.00’
16.50’
14°S
17.00’
17.50’
18.00’
42’
41’
170°W
40.00’
39’
38’

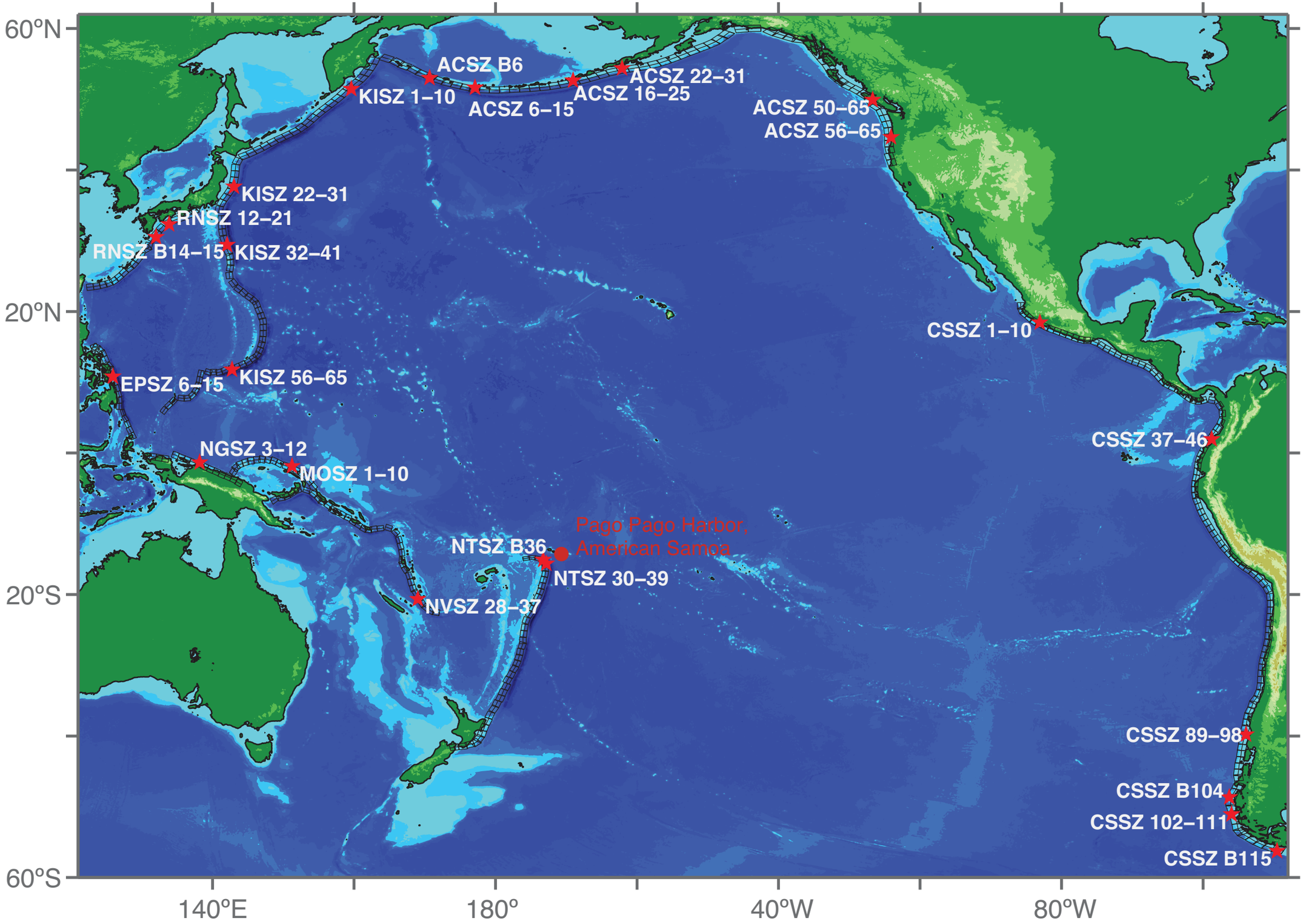
60°N
20°N
20°S
60°S
140°E
180°
40°W
80°W
ACSZ B6
KISZ 1–10
ACSZ 6–15
ACSZ 22–31
ACSZ 16–25
ACSZ 50–65
ACSZ 56–65
KISZ 22–31
RNSZ 12–21
RNSZ B14–15
KISZ 32–41
CSSZ 1–10
EPSZ 6–15
KISZ 56–65
CSSZ 37–46
NGSZ 3–12
MOSZ 1–10
Pago Pago Harbor,
American Samoa
NTSZ B36
NTSZ 30–39
NVSZ 28–37
CSSZ 89–98
CSSZ B104
CSSZ 102–111
CSSZ B115

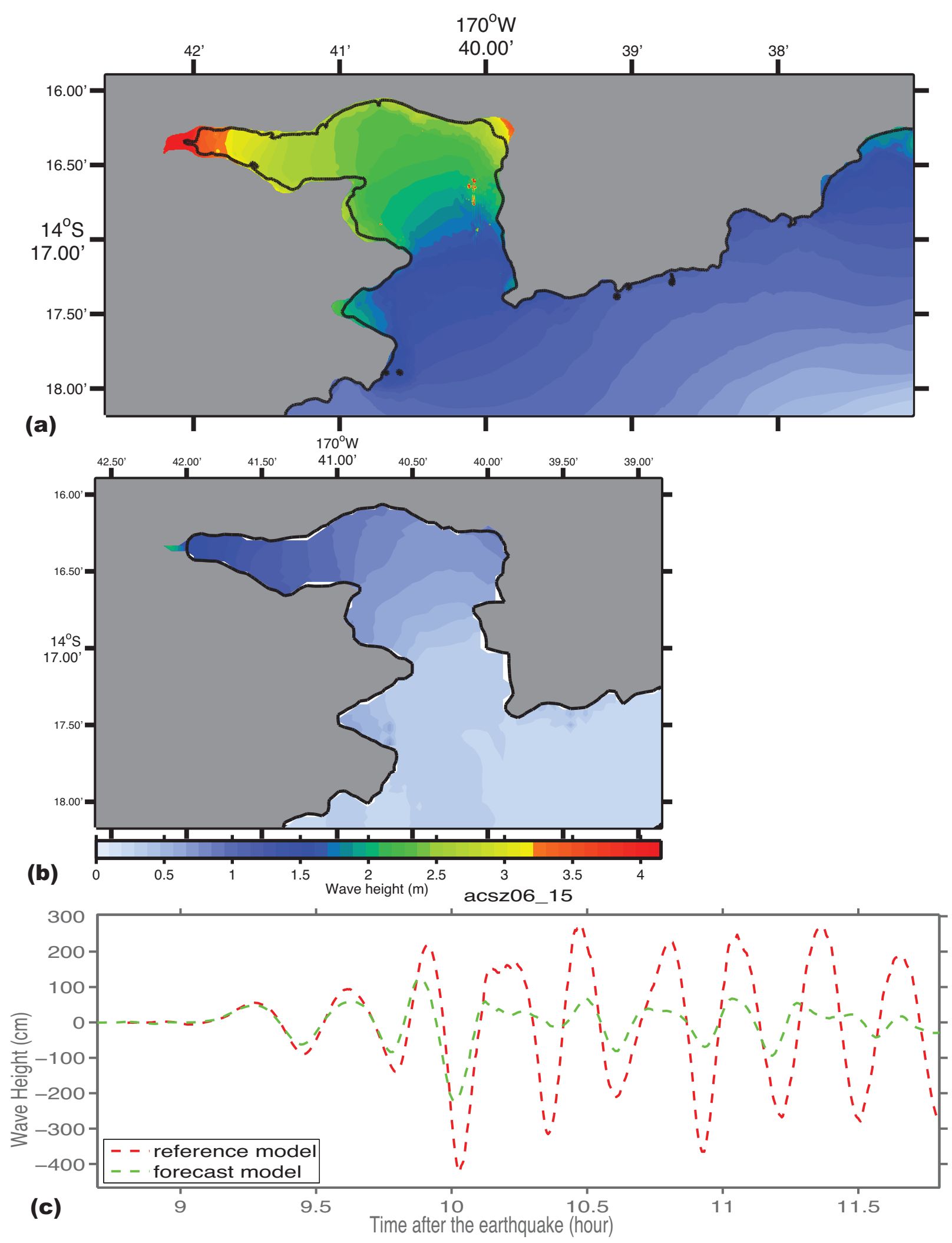
170°W
40.00'
42'
41'
39'
38'
16.00'
16.50'
14°S
17.00'
17.50'
18.00'
(a)
170°W
41.00'
42.50'
42.00'
41.50'
40.50'
40.00'
39.50'
39.00'
16.00'
16.50'
14°S
17.00'
17.50'
18.00'
0
0.5
1
1.5
2
2.5
3
3.5
4
Wave height (m)
(b)
acsz06_15
300
200
100
0
−100
−200
−300
−400
Wave Height (cm)
reference model
forecast model
9
9.5
10
10.5
11
11.5
Time after the earthquake (hour)
(c)

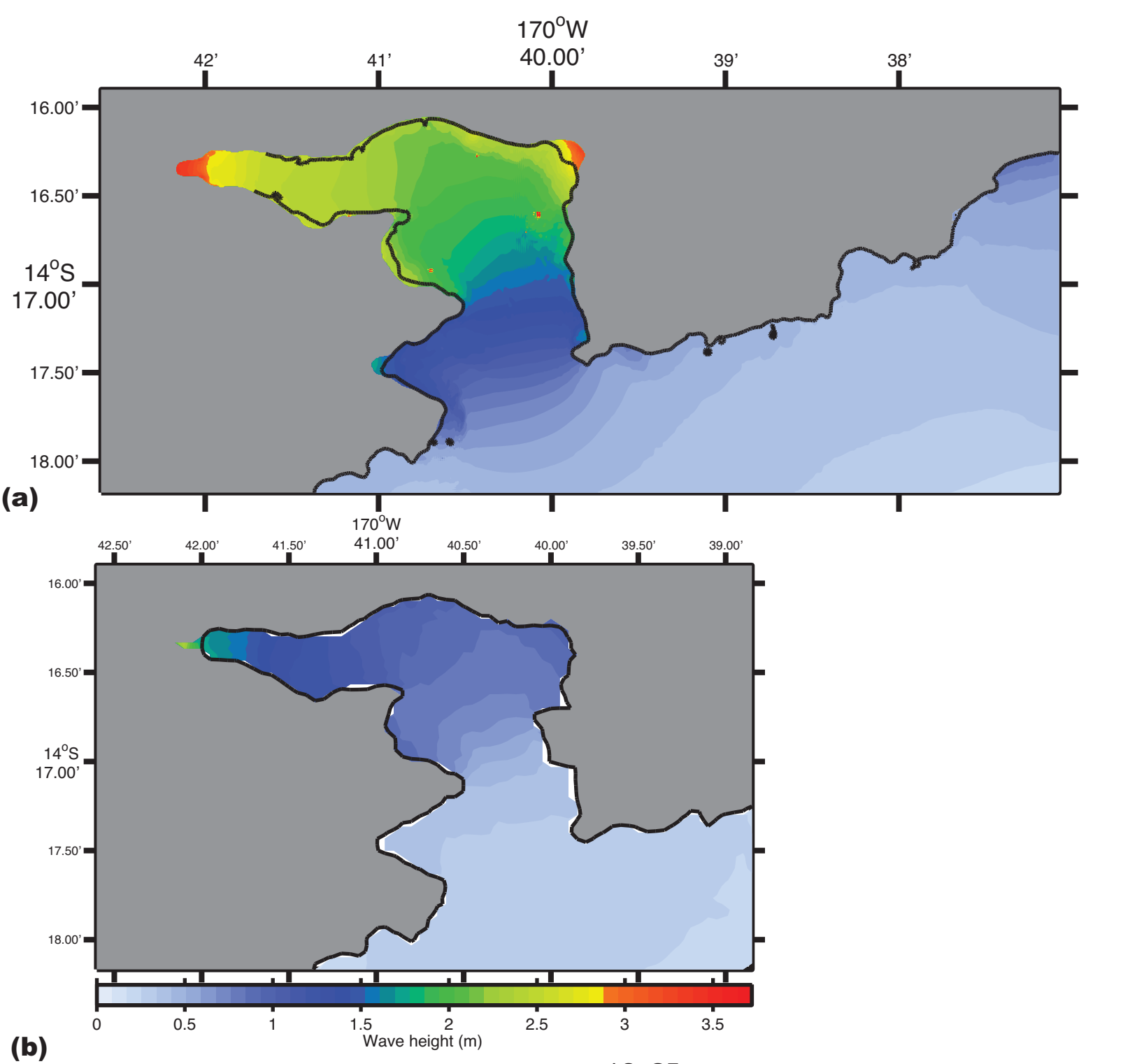
170°W
40.00'
42'
41'
39'
38'
16.00'
16.50'
14°S
17.00'
17.50'
18.00'
(a)

170°W
41.00'
42.50'
42.00'
41.50'
40.50'
40.00'
39.50'
39.00'
16.00'
16.50'
14°S
17.00'
17.50'
18.00'
0
0.5
1
1.5
2
2.5
3
3.5
Wave height (m)
(b)

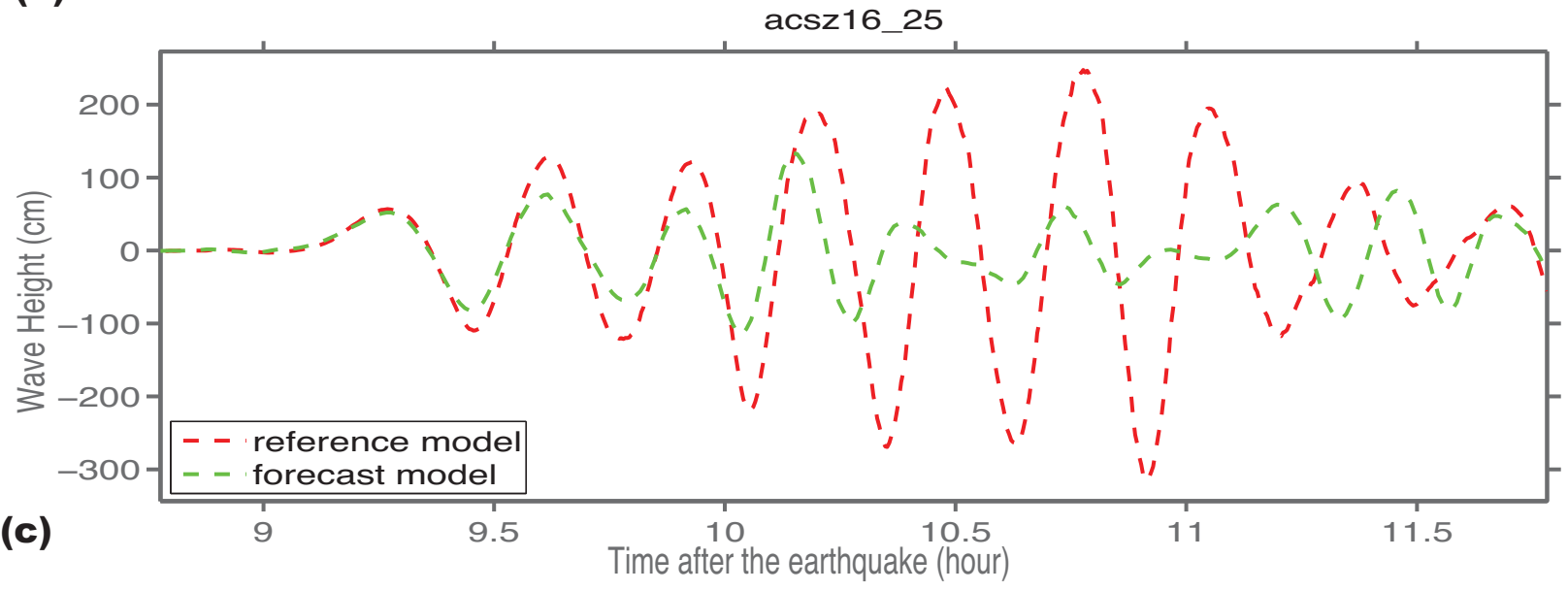
acsz16_25
200
100
0
−100
−200
−300
Wave Height (cm)
reference model
forecast model
9
9.5
10
10.5
11
11.5
Time after the earthquake (hour)
(c)

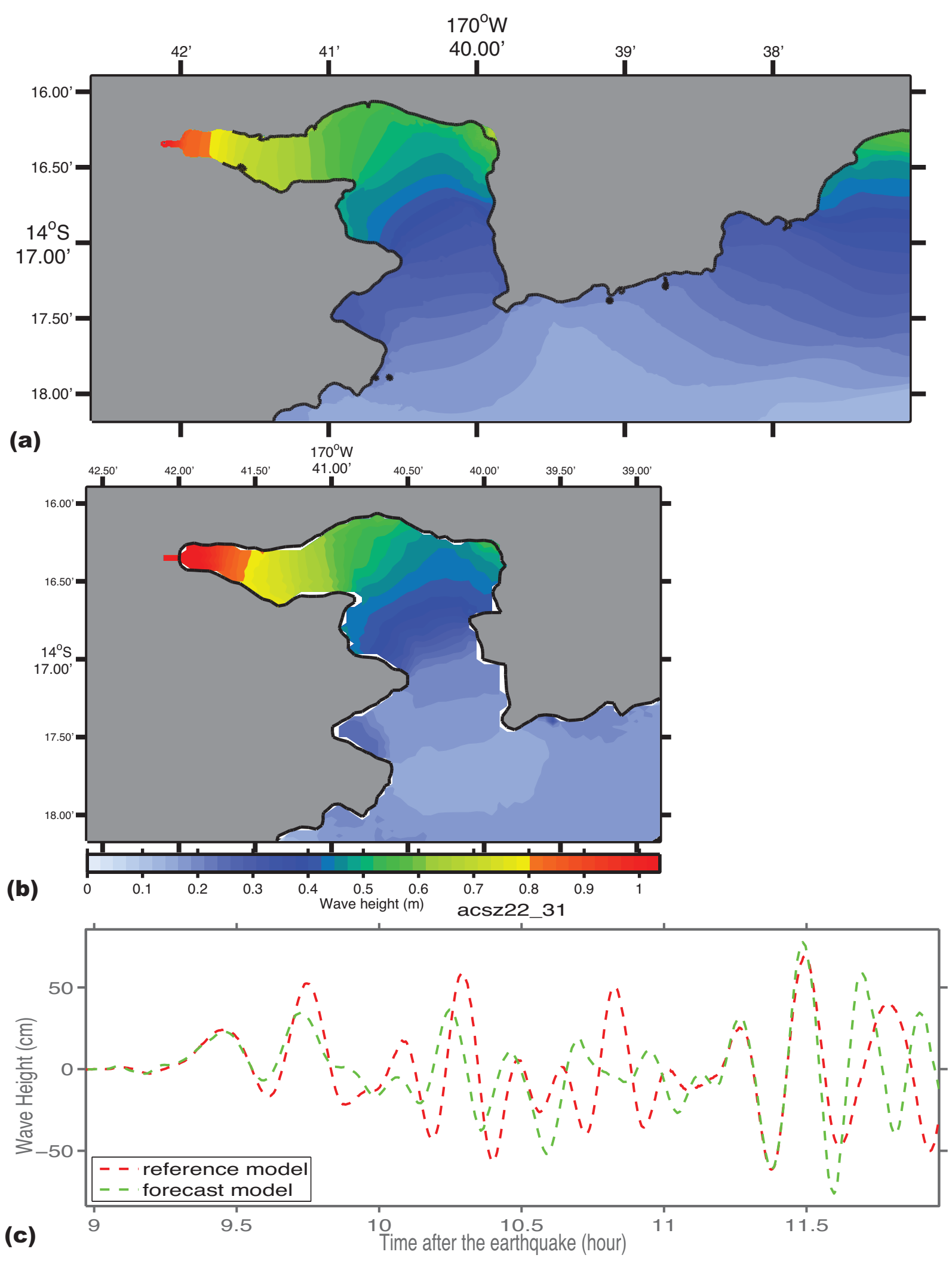
170°W
40.00'
42'
41'
39'
38'
16.00'
16.50'
14°S
17.00'
17.50'
18.00'
(a)
170°W
41.00'
42.50'
42.00'
41.50'
40.50'
40.00'
39.50'
39.00'
16.00'
16.50'
14°S
17.00'
17.50'
18.00'
0
0.1
0.2
0.3
0.4
0.5
0.6
0.7
0.8
0.9
1
Wave height (m)
(b)
acsz22_31
50
0
−50
Wave Height (cm)
reference model
forecast model
9
9.5
10
10.5
11
11.5
Time after the earthquake (hour)
(c)

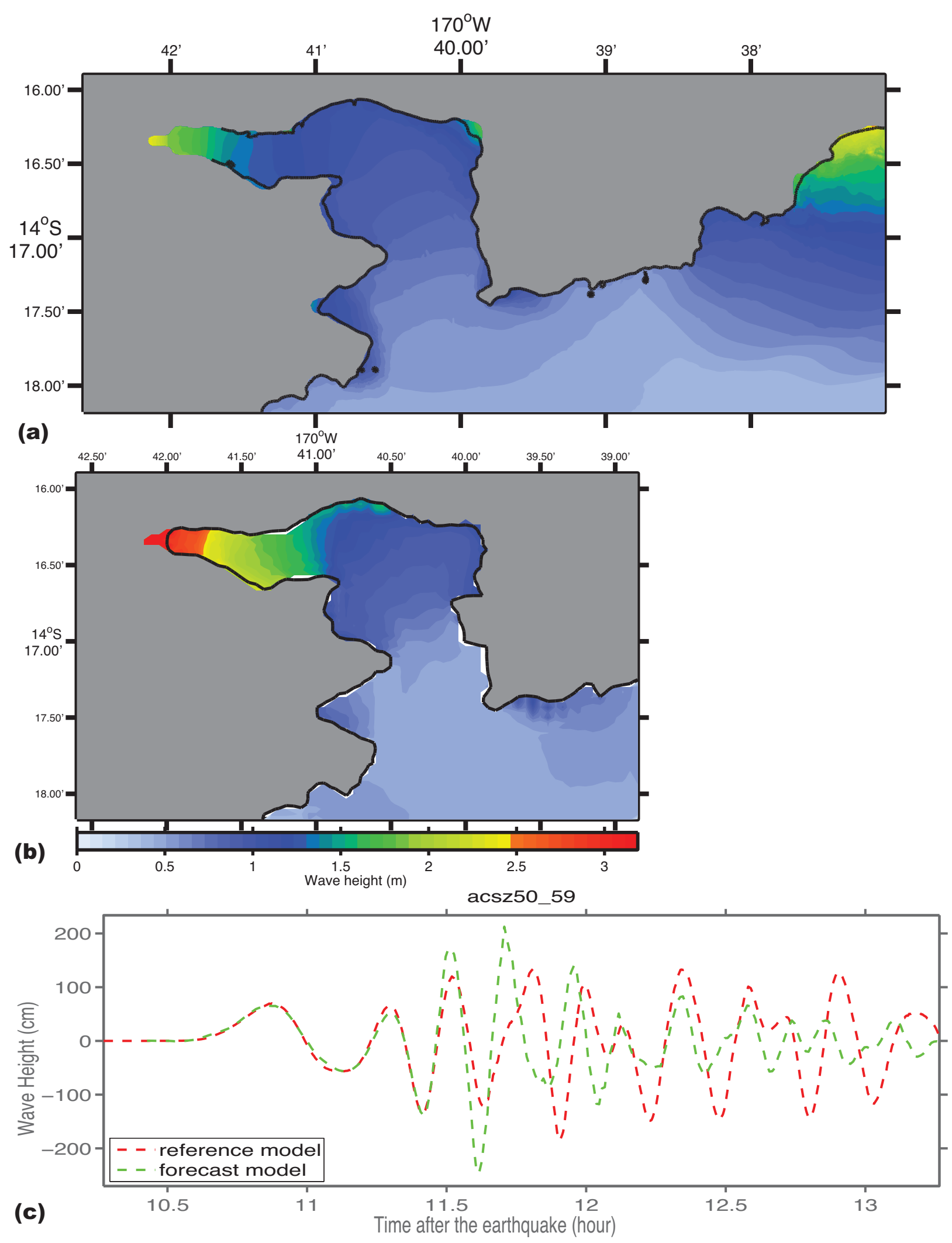
170°W
40.00'
42'
41'
39'
38'
16.00'
16.50'
14°S
17.00'
17.50'
18.00'
(a)
170°W
41.00'
42.50'
42.00'
41.50'
40.50'
40.00'
39.50'
39.00'
16.00'
16.50'
14°S
17.00'
17.50'
18.00'
(b)
0
0.5
1
1.5
2
2.5
3
Wave height (m)
acsz50_59
200
100
0
−100
−200
Wave Height (cm)
reference model
forecast model
10.5
11
11.5
12
12.5
13
Time after the earthquake (hour)
(c)

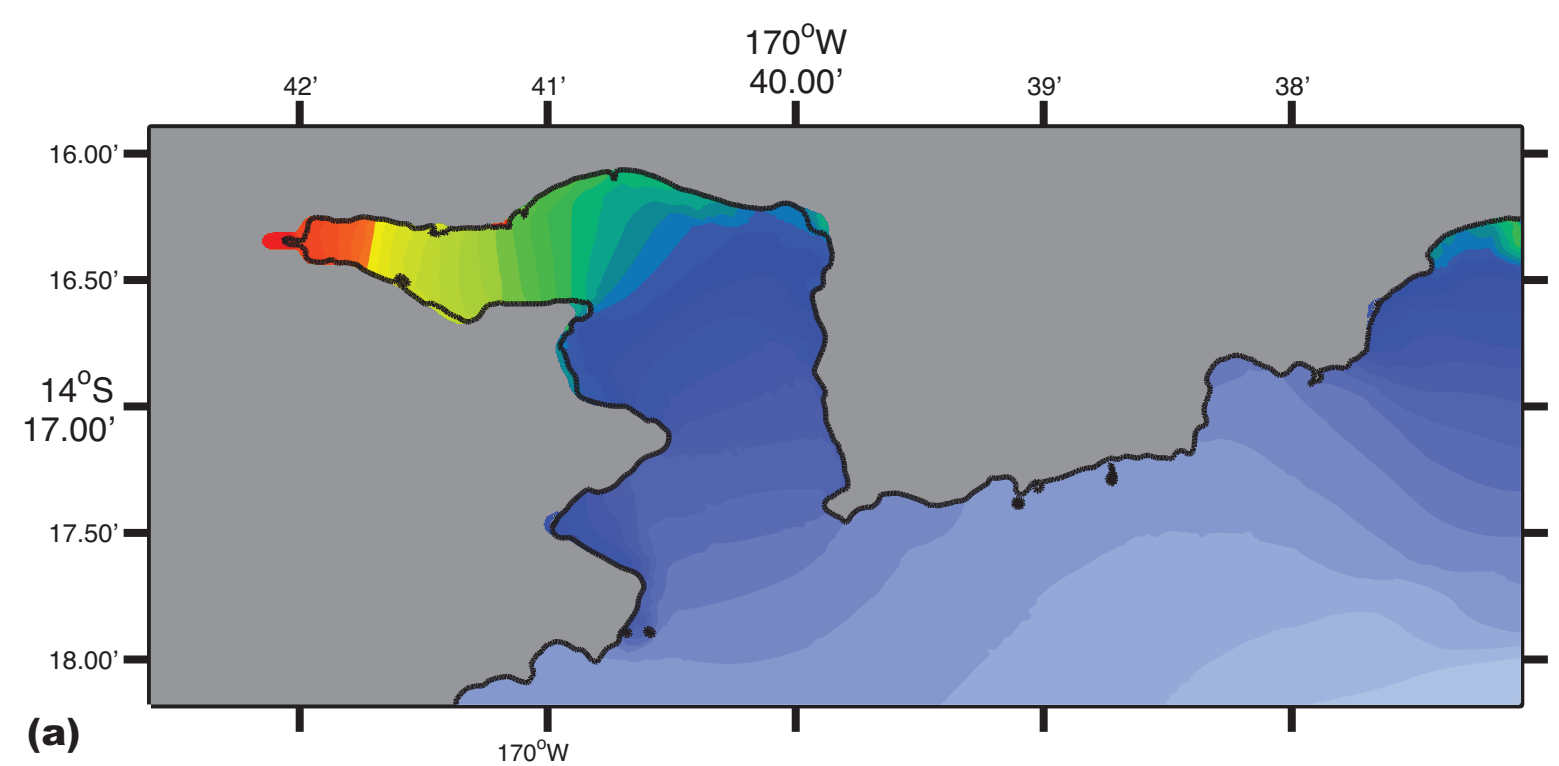
170°W
40.00'
42'
41'
39'
38'
16.00'
16.50'
14°S
17.00'
17.50'
18.00'

(a)

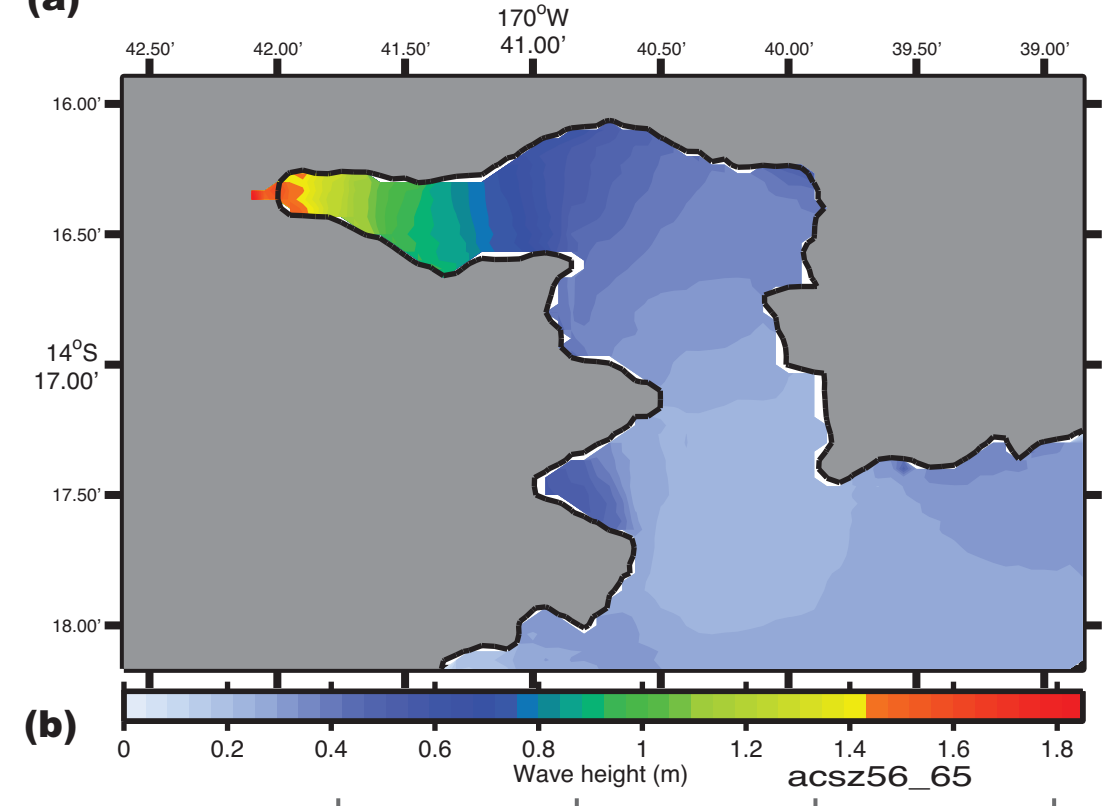
170°W
41.00'
42.50'
42.00'
41.50'
40.50'
40.00'
39.50'
39.00'
16.00'
16.50'
14°S
17.00'
17.50'
18.00'
0
0.2
0.4
0.6
0.8
1
1.2
1.4
1.6
1.8
Wave height (m)
acsz56_65

(b)

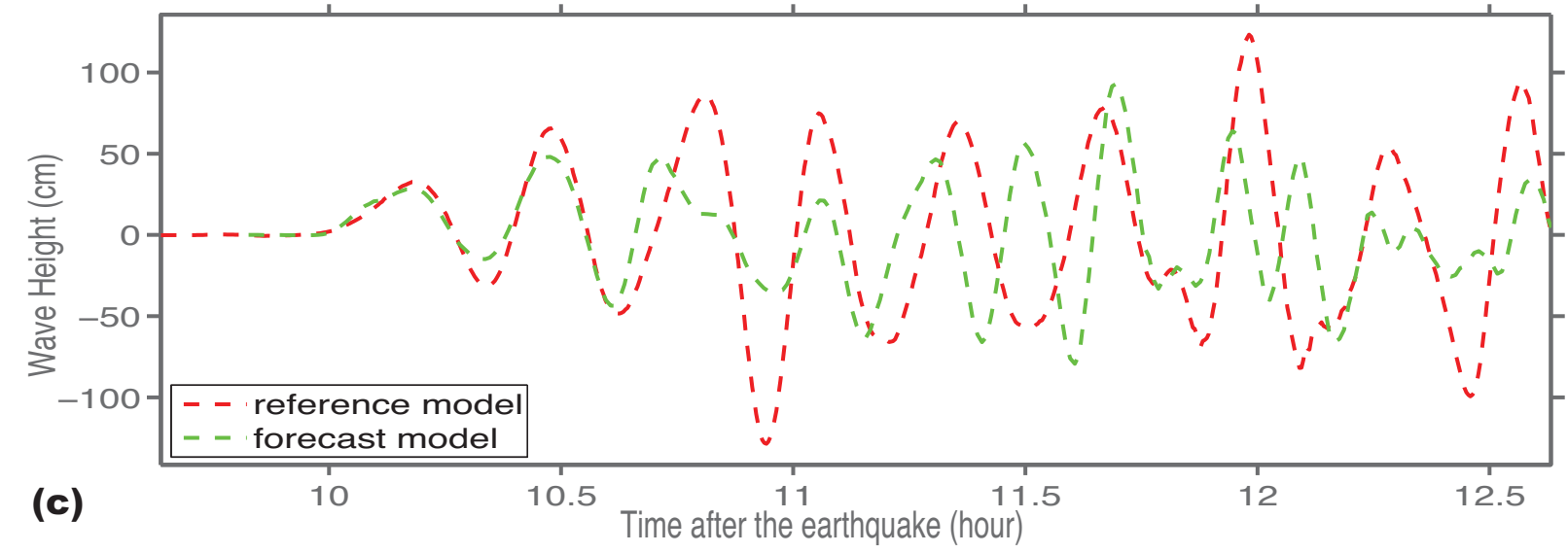
100
50
0
−50
−100
Wave Height (cm)
reference model
forecast model
10
10.5
11
11.5
12
12.5
Time after the earthquake (hour)

(c)

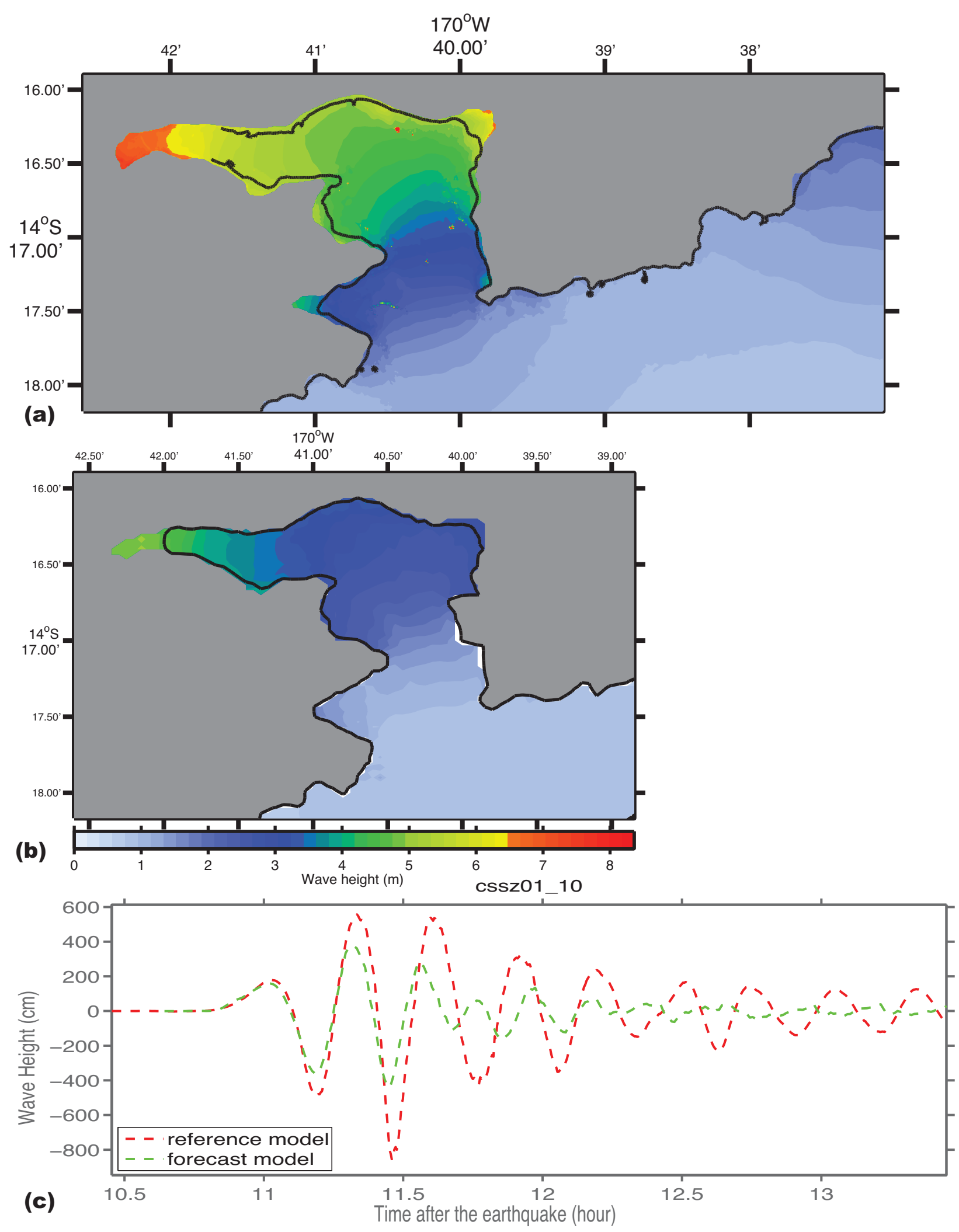
170°W
40.00'
42'
41'
39'
38'
16.00'
16.50'
14°S
17.00'
17.50'
18.00'
(a)
170°W
41.00'
42.50'
42.00'
41.50'
40.50'
40.00'
39.50'
39.00'
16.00'
16.50'
14°S
17.00'
17.50'
18.00'
(b)
0
1
2
3
4
5
6
7
8
Wave height (m)
cssz01_10
600
400
200
0
−200
−400
−600
−800
Wave Height (cm)
reference model
forecast model
10.5
11
11.5
12
12.5
13
Time after the earthquake (hour)
(c)

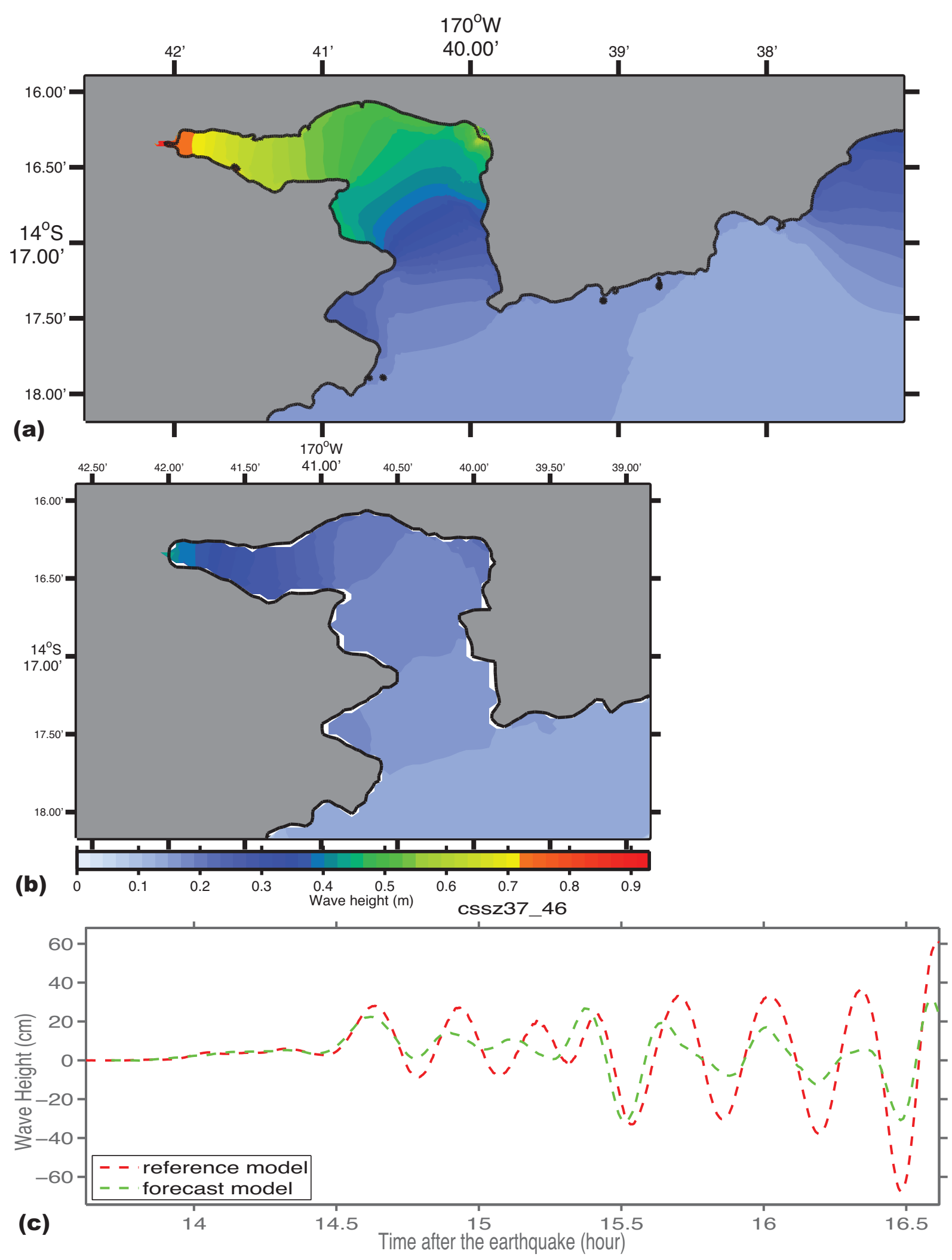
170°W
40.00'
42'
41'
39'
38'
16.00'
16.50'
14°S
17.00'
17.50'
18.00'
(a)
170°W
41.00'
42.50'
42.00'
41.50'
40.50'
40.00'
39.50'
39.00'
16.00'
16.50'
14°S
17.00'
17.50'
18.00'
0
0.1
0.2
0.3
0.4
0.5
0.6
0.7
0.8
0.9
Wave height (m)
(b)
cssz37_46
60
40
20
0
−20
−40
−60
Wave Height (cm)
reference model
forecast model
14
14.5
15
15.5
16
16.5
Time after the earthquake (hour)
(c)

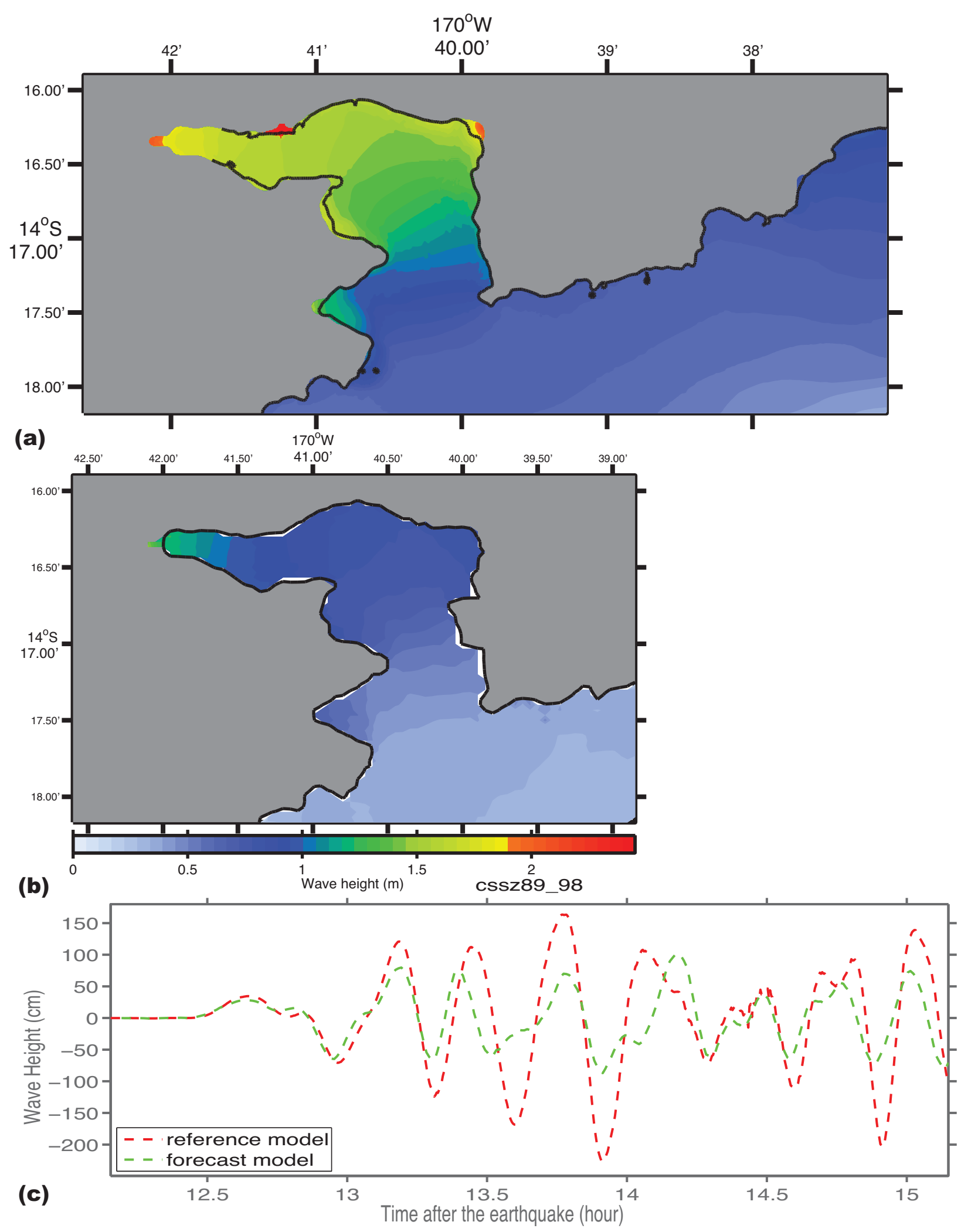
170°W
40.00'
42'
41'
39'
38'
16.00'
16.50'
14°S
17.00'
17.50'
18.00'
(a)
170°W
41.00'
42.50'
42.00'
41.50'
40.50'
40.00'
39.50'
39.00'
16.00'
16.50'
14°S
17.00'
17.50'
18.00'
0
0.5
1
1.5
2
Wave height (m)
(b)
cssz89_98
150
100
50
0
−50
−100
−150
−200
Wave Height (cm)
reference model
forecast model
12.5
13
13.5
14
14.5
15
Time after the earthquake (hour)
(c)

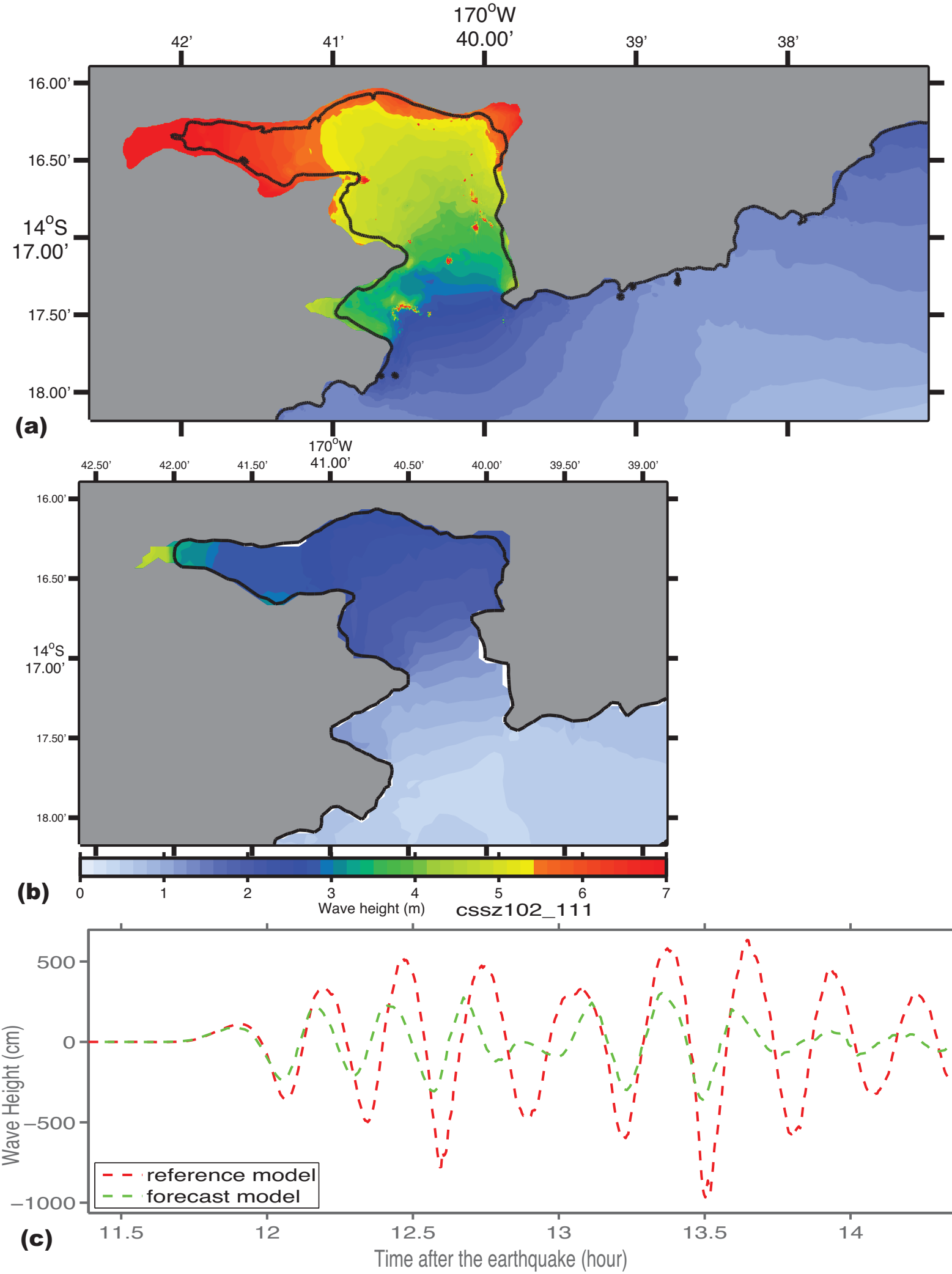
170°W
40.00'
42'
41'
39'
38'
16.00'
16.50'
14°S
17.00'
17.50'
18.00'
(a)
170°W
41.00'
42.50'
42.00'
41.50'
40.50'
40.00'
39.50'
39.00'
16.00'
16.50'
14°S
17.00'
17.50'
18.00'
0
1
2
3
4
5
6
7
Wave height (m)
(b)
cssz102_111
500
0
−500
−1000
Wave Height (cm)
reference model
forecast model
11.5
12
12.5
13
13.5
14
Time after the earthquake (hour)
(c)

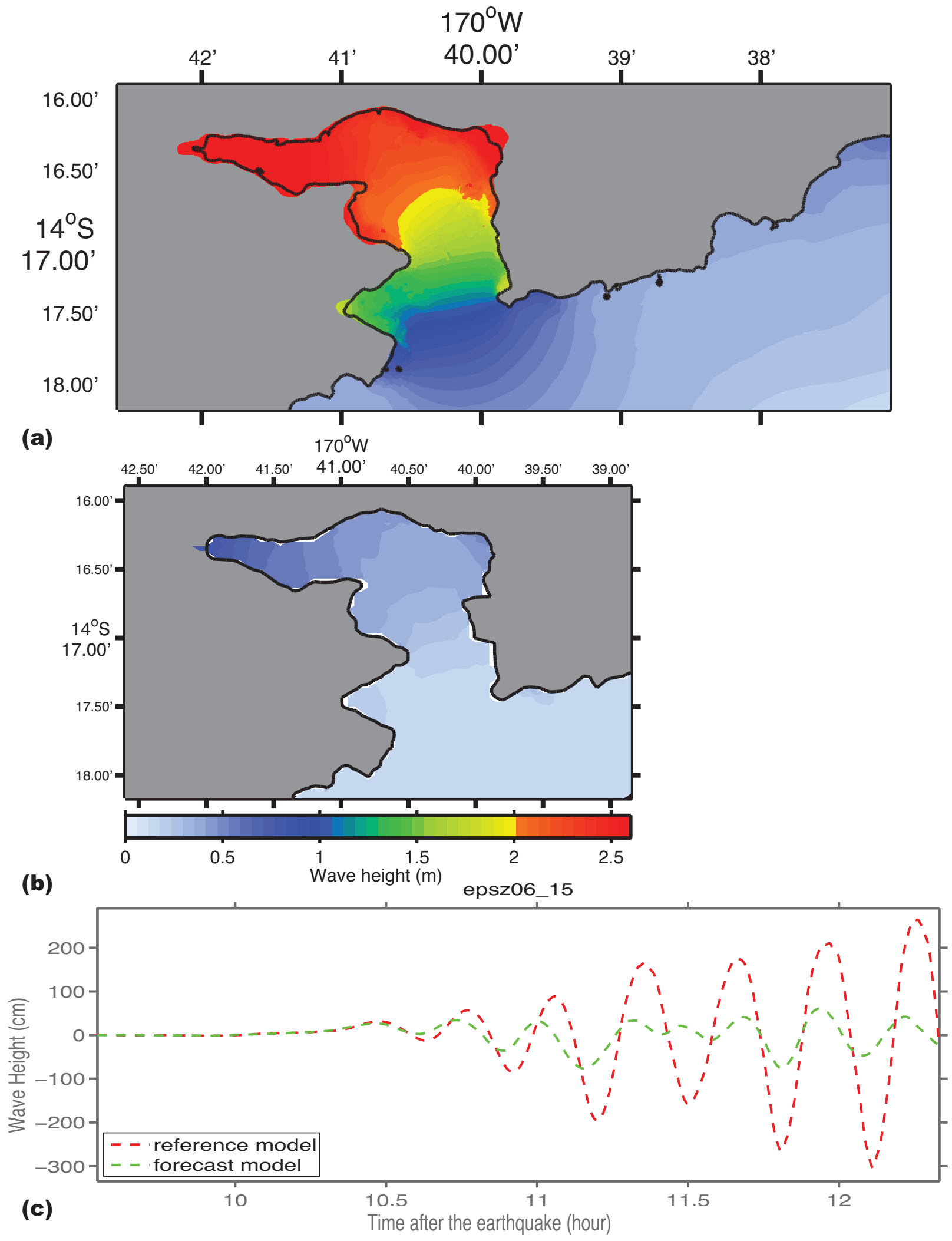
170°W
40.00'
42'
41'
39'
38'
16.00'
16.50'
14°S
17.00'
17.50'
18.00'
(a)
170°W
41.00'
42.50'
42.00'
41.50'
40.50'
40.00'
39.50'
39.00'
16.00'
16.50'
14°S
17.00'
17.50'
18.00'
0
0.5
1
1.5
2
2.5
Wave height (m)
(b)
epsz06_15
200
100
0
−100
−200
−300
Wave Height (cm)
reference model
forecast model
10
10.5
11
11.5
12
Time after the earthquake (hour)
(c)

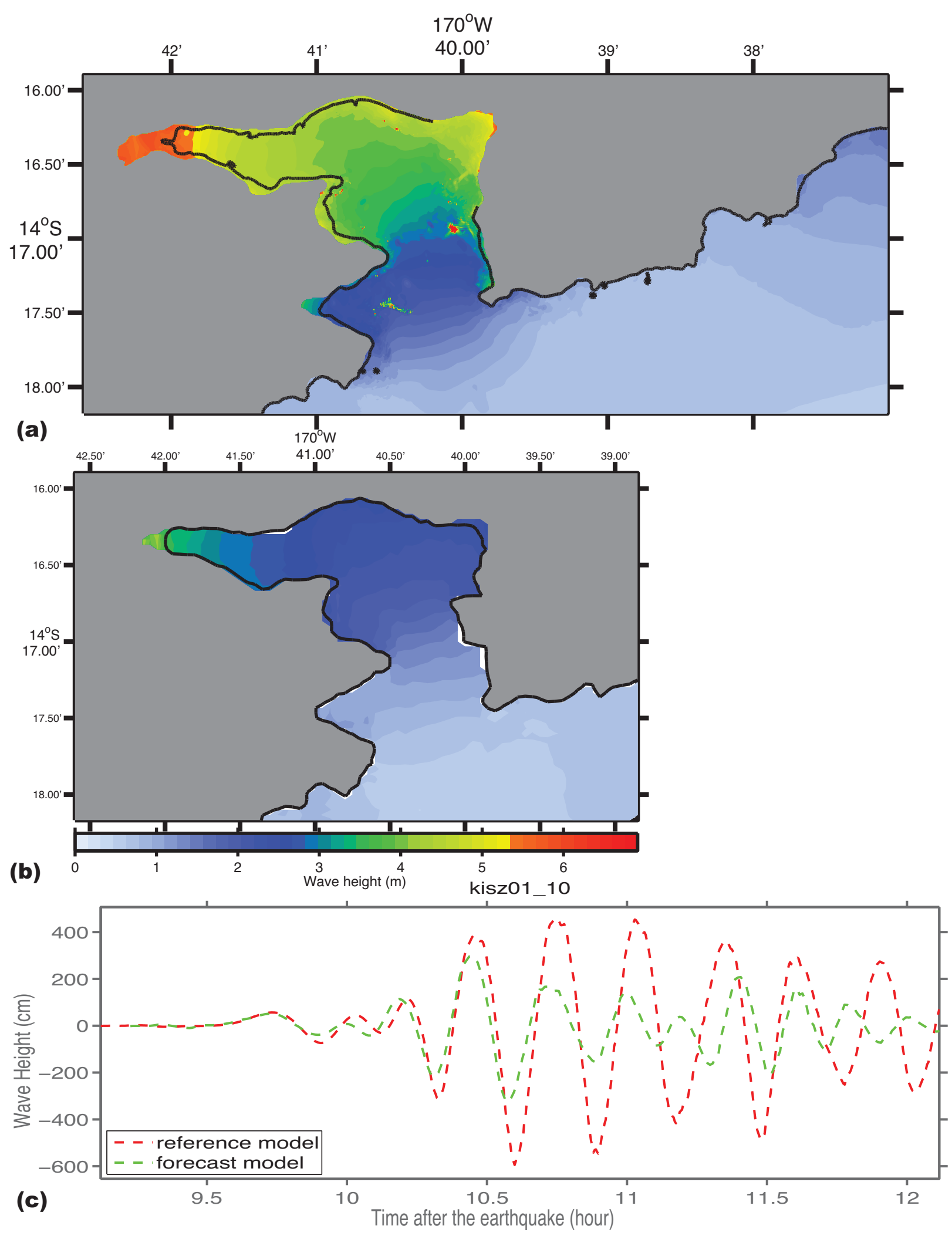
170°W
40.00'
42'
41'
39'
38'
16.00'
16.50'
14°S
17.00'
17.50'
18.00'
(a)
170°W
41.00'
42.50'
42.00'
41.50'
40.50'
40.00'
39.50'
39.00'
16.00'
16.50'
14°S
17.00'
17.50'
18.00'
0
1
2
3
4
5
6
Wave height (m)
(b)
kisz01_10
400
200
0
−200
−400
−600
Wave Height (cm)
reference model
forecast model
9.5
10
10.5
11
11.5
12
Time after the earthquake (hour)
(c)

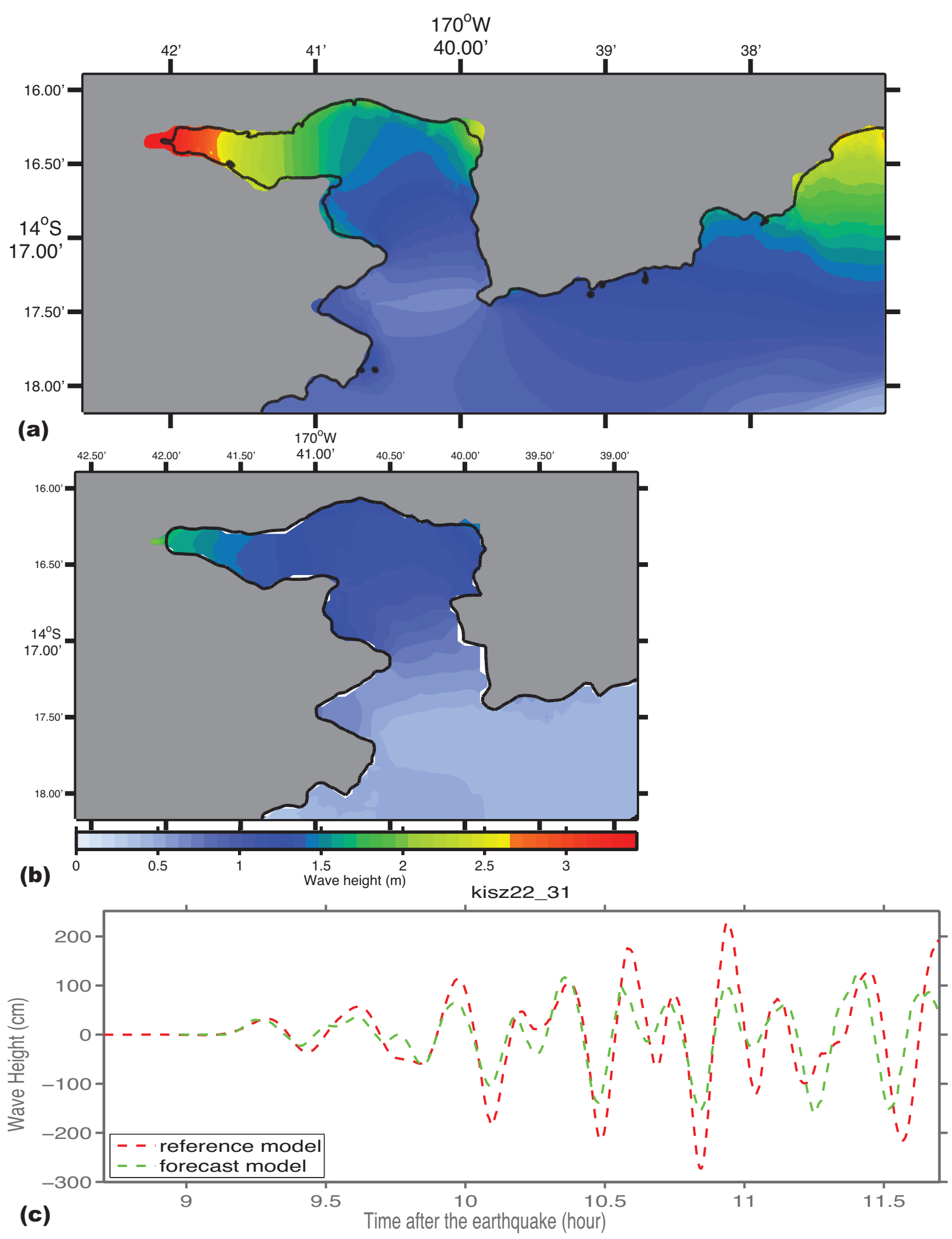
170°W
40.00'
42'
41'
39'
38'
16.00'
16.50'
14°S
17.00'
17.50'
18.00'
(a)
170°W
41.00'
42.50'
42.00'
41.50'
40.50'
40.00'
39.50'
39.00'
16.00'
16.50'
14°S
17.00'
17.50'
18.00'
0
0.5
1
1.5
2
2.5
3
Wave height (m)
(b)
kisz22_31
200
100
0
−100
−200
−300
Wave Height (cm)
reference model
forecast model
9
9.5
10
10.5
11
11.5
Time after the earthquake (hour)
(c)

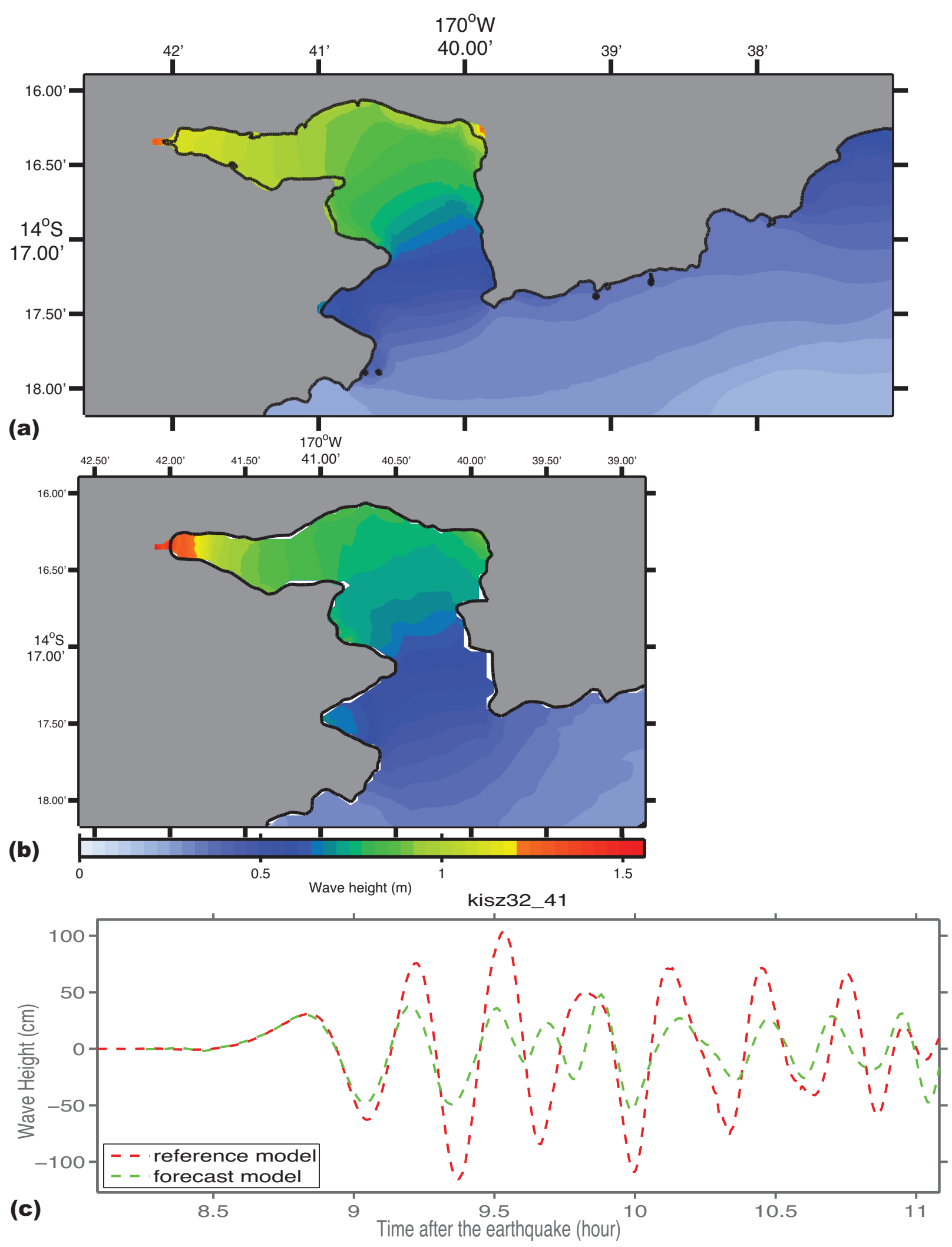
170°W
40.00'
42'
41'
39'
38'
16.00'
16.50'
14°S
17.00'
17.50'
18.00'
(a)
170°W
41.00'
42.50'
42.00'
41.50'
40.50'
40.00'
39.50'
39.00'
16.00'
16.50'
14°S
17.00'
17.50'
18.00'
(b)
0
0.5
1
1.5
Wave height (m)
kisz32_41
100
50
0
−50
−100
Wave Height (cm)
reference model
forecast model
8.5
9
9.5
10
10.5
11
Time after the earthquake (hour)
(c)

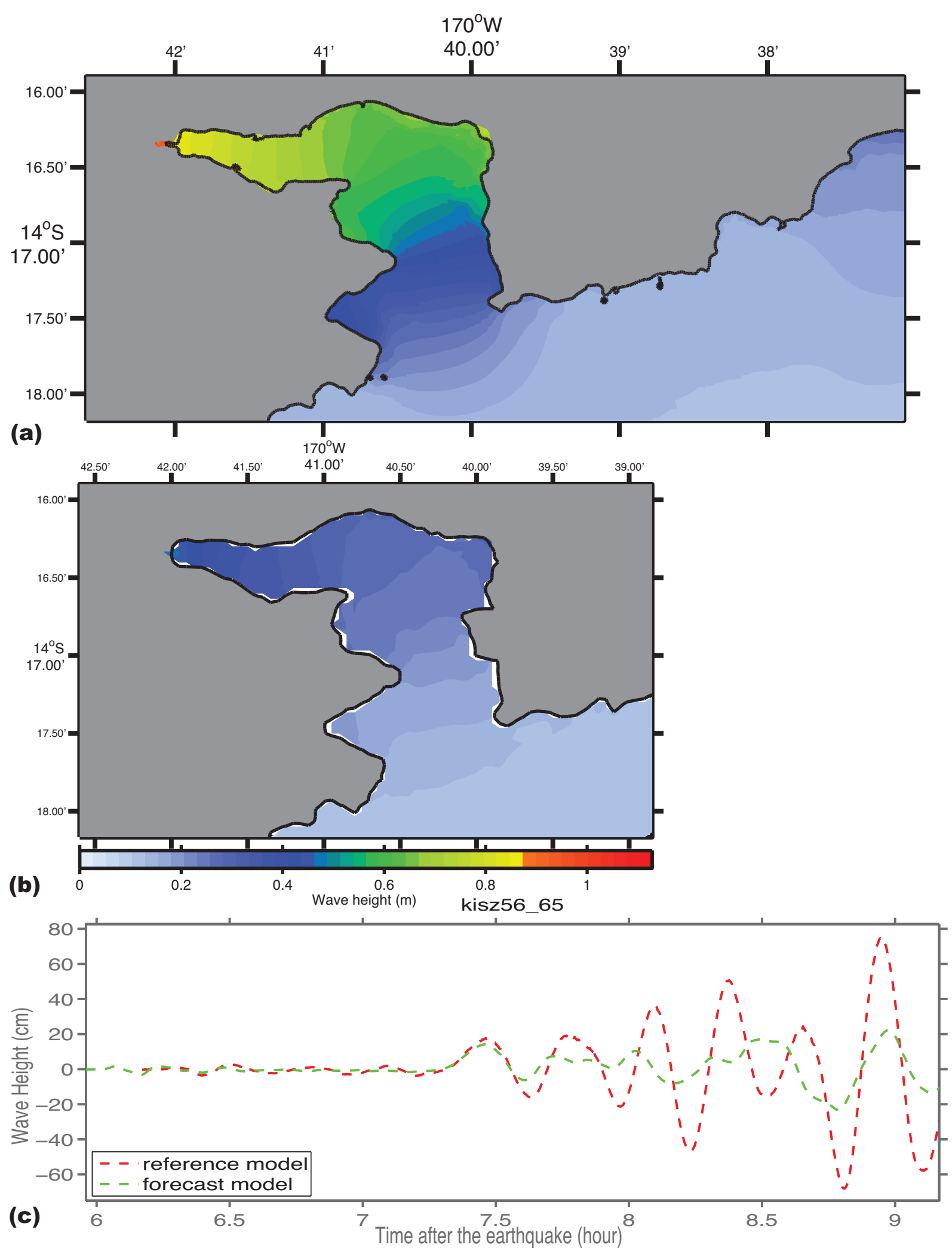
170°W
40.00'
42'
41'
39'
38'
16.00'
16.50'
14°S
17.00'
17.50'
18.00'
(a)
170°W
41.00'
42.50'
42.00'
41.50'
40.50'
40.00'
39.50'
39.00'
16.00'
16.50'
14°S
17.00'
17.50'
18.00'
0
0.2
0.4
0.6
0.8
1
Wave height (m)
(b)
kisz56_65
80
60
40
20
0
−20
−40
−60
Wave Height (cm)
reference model
forecast model
6
6.5
7
7.5
8
8.5
9
Time after the earthquake (hour)
(c)

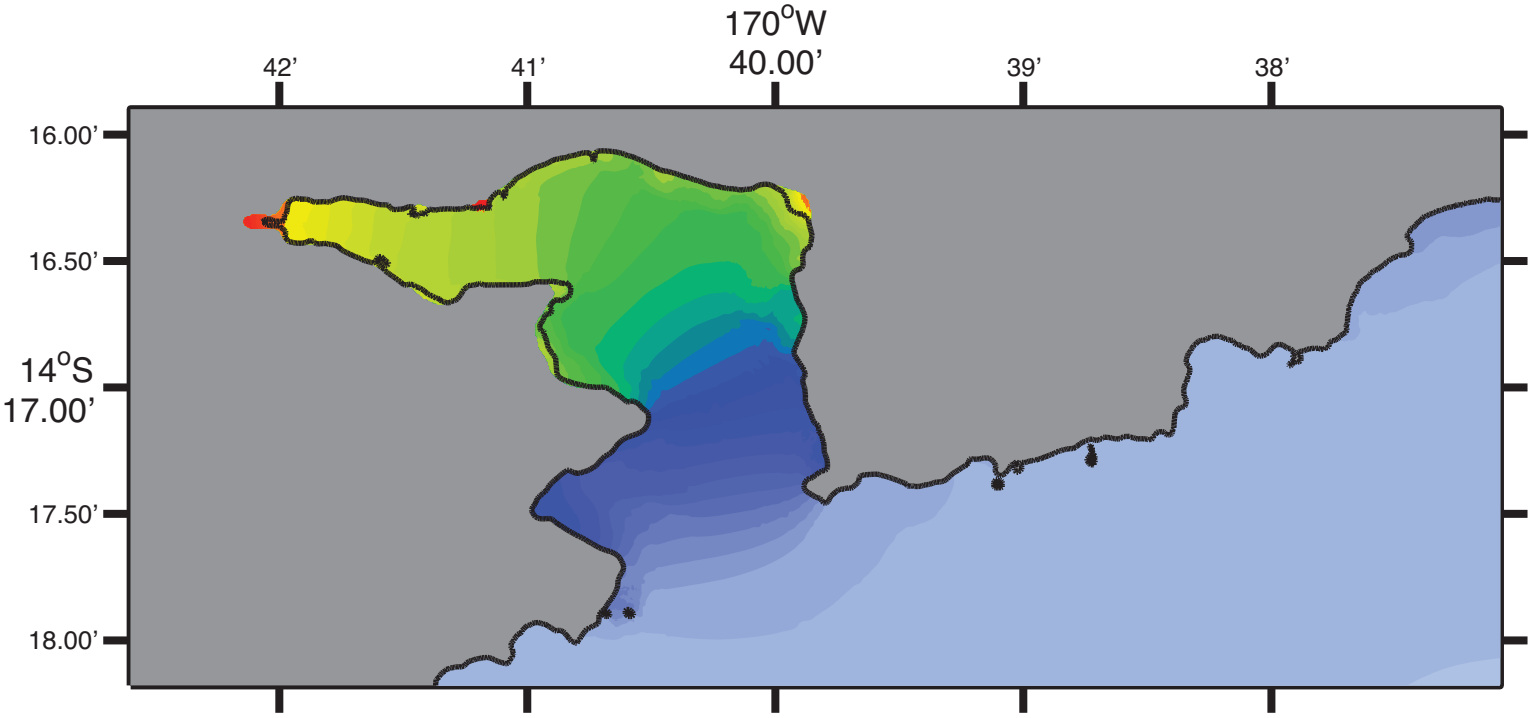
170°W
40.00'
42'
41'
39'
38'
16.00'
16.50'
14°S
17.00'
17.50'
18.00'

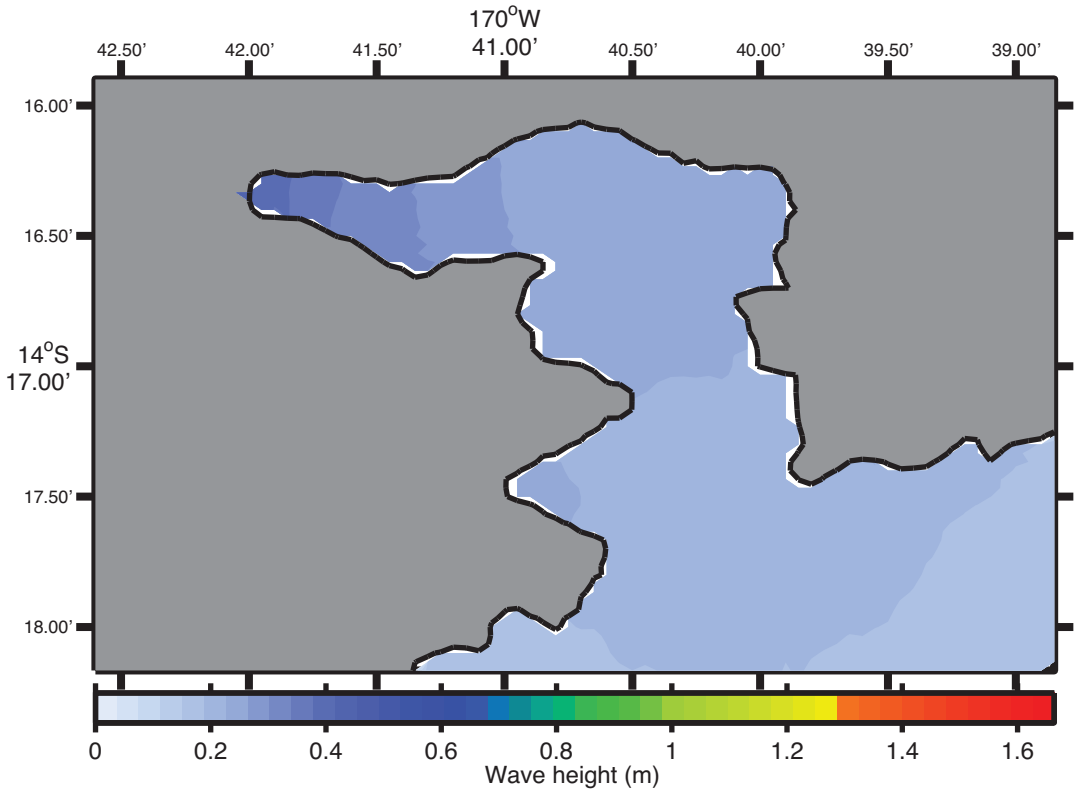
170°W
41.00'
42.50'
42.00'
41.50'
40.50'
40.00'
39.50'
39.00'
16.00'
16.50'
14°S
17.00'
17.50'
18.00'
0
0.2
0.4
0.6
0.8
1
1.2
1.4
1.6
Wave height (m)

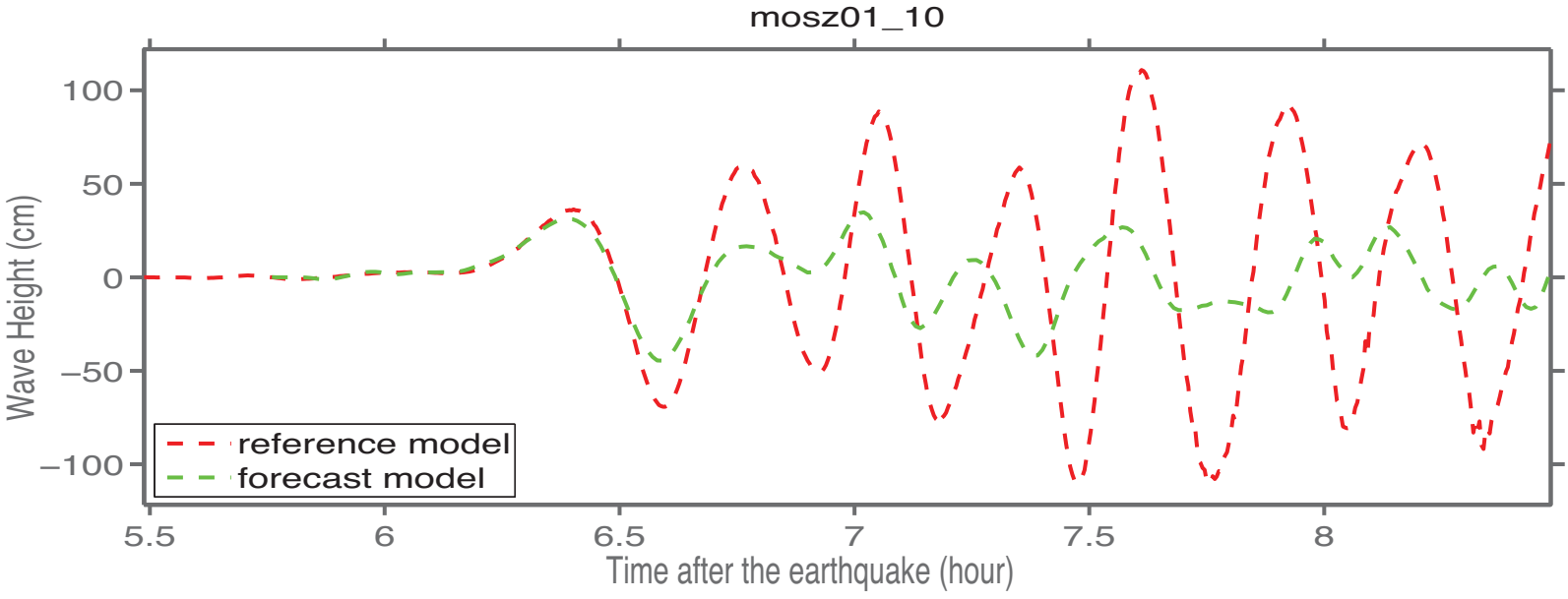
mosz01_10
100
50
0
−50
−100
Wave Height (cm)
reference model
forecast model
5.5
6
6.5
7
7.5
8
Time after the earthquake (hour)

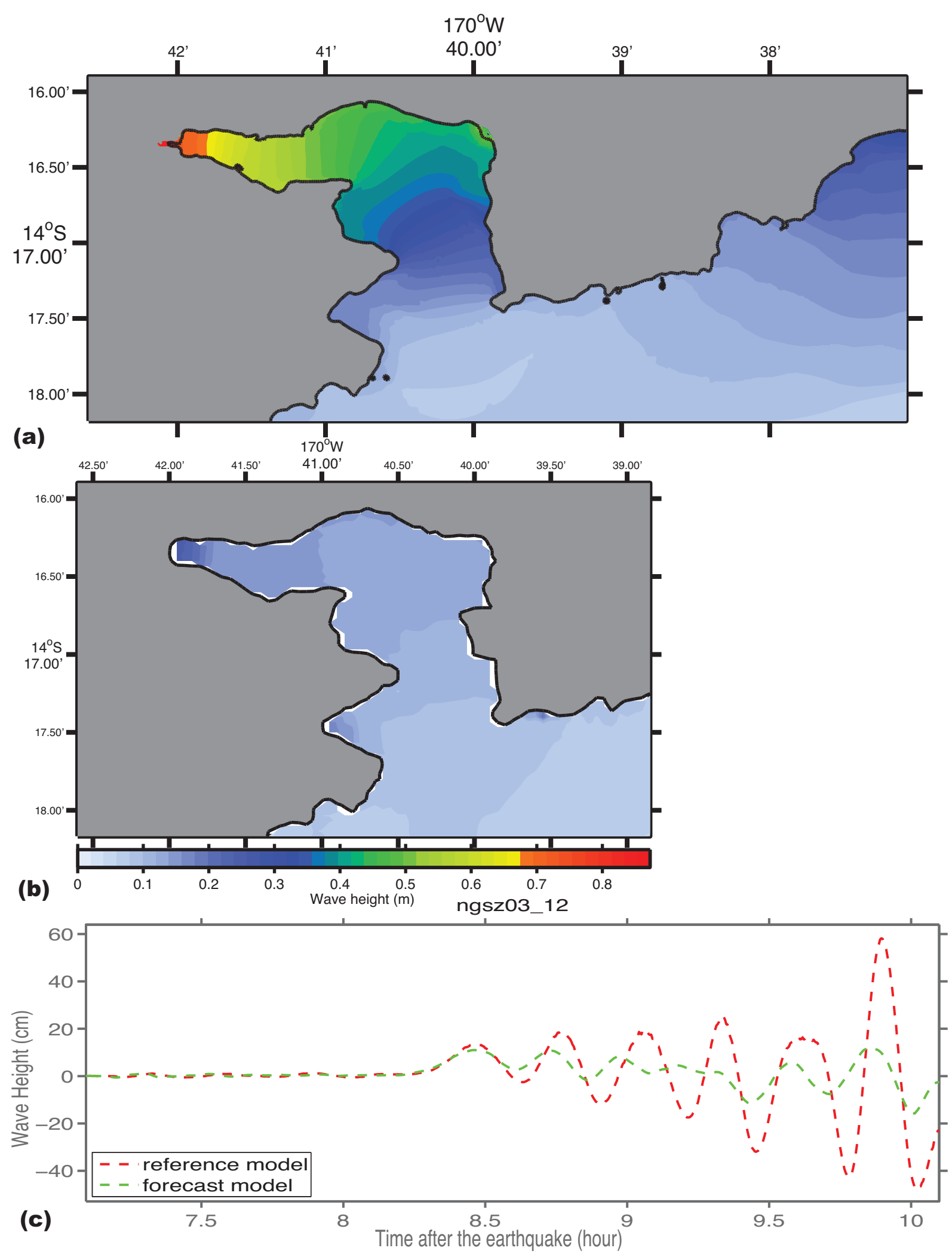
170°W
40.00'
42'
41'
39'
38'
16.00'
16.50'
14°S
17.00'
17.50'
18.00'
(a)
170°W
41.00'
42.50'
42.00'
41.50'
40.50'
40.00'
39.50'
39.00'
16.00'
16.50'
14°S
17.00'
17.50'
18.00'
0
0.1
0.2
0.3
0.4
0.5
0.6
0.7
0.8
Wave height (m)
(b)
ngsz03_12
60
40
20
0
−20
−40
Wave Height (cm)
reference model
forecast model
7.5
8
8.5
9
9.5
10
Time after the earthquake (hour)
(c)

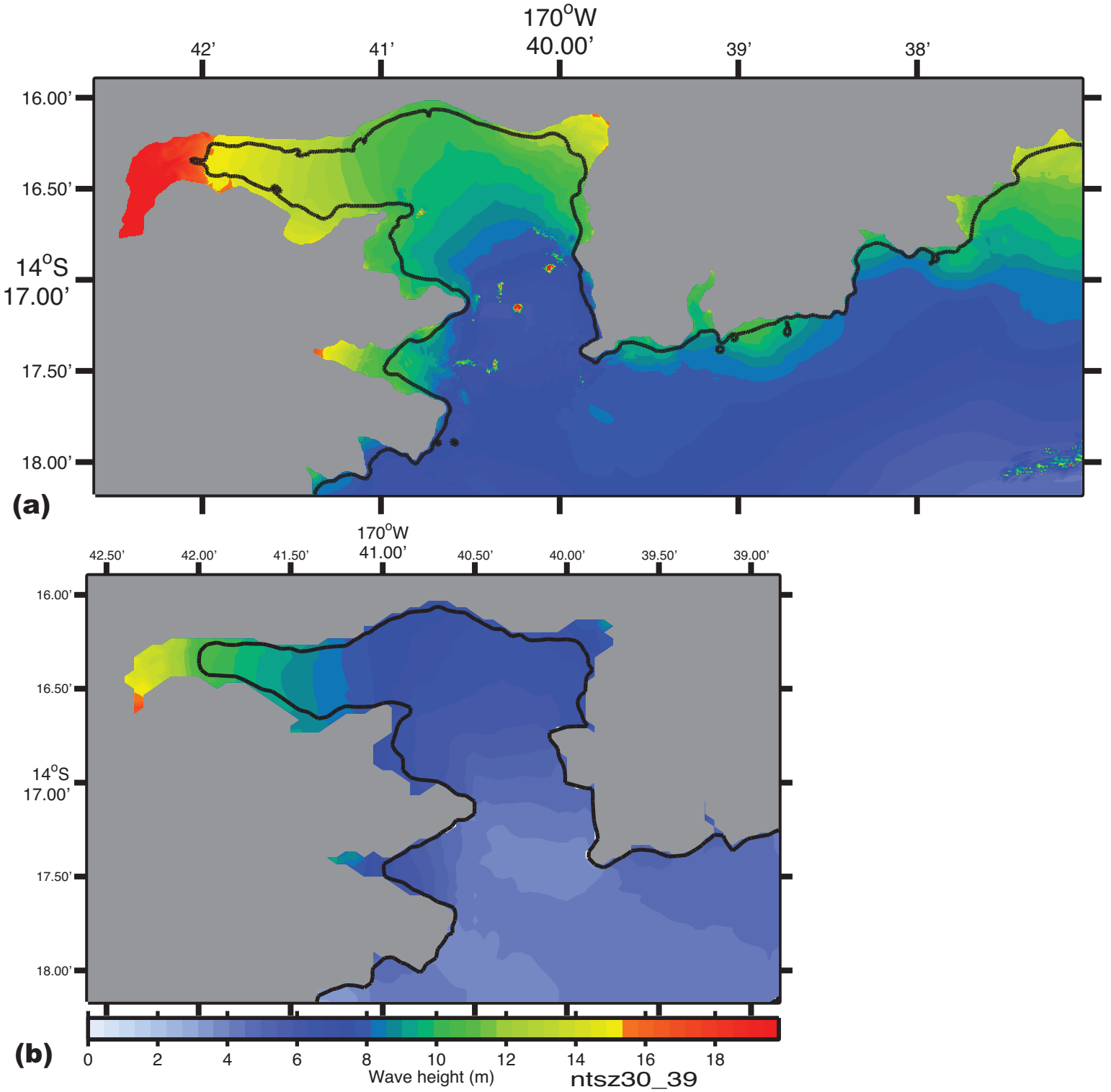
170°W
40.00'
42'
41'
39'
38'
16.00'
16.50'
14°S
17.00'
17.50'
18.00'
(a)

170°W
41.00'
42.50'
42.00'
41.50'
40.50'
40.00'
39.50'
39.00'
16.00'
16.50'
14°S
17.00'
17.50'
18.00'
(b)
0
2
4
6
8
10
12
14
16
18
Wave height (m)
ntsz30_39

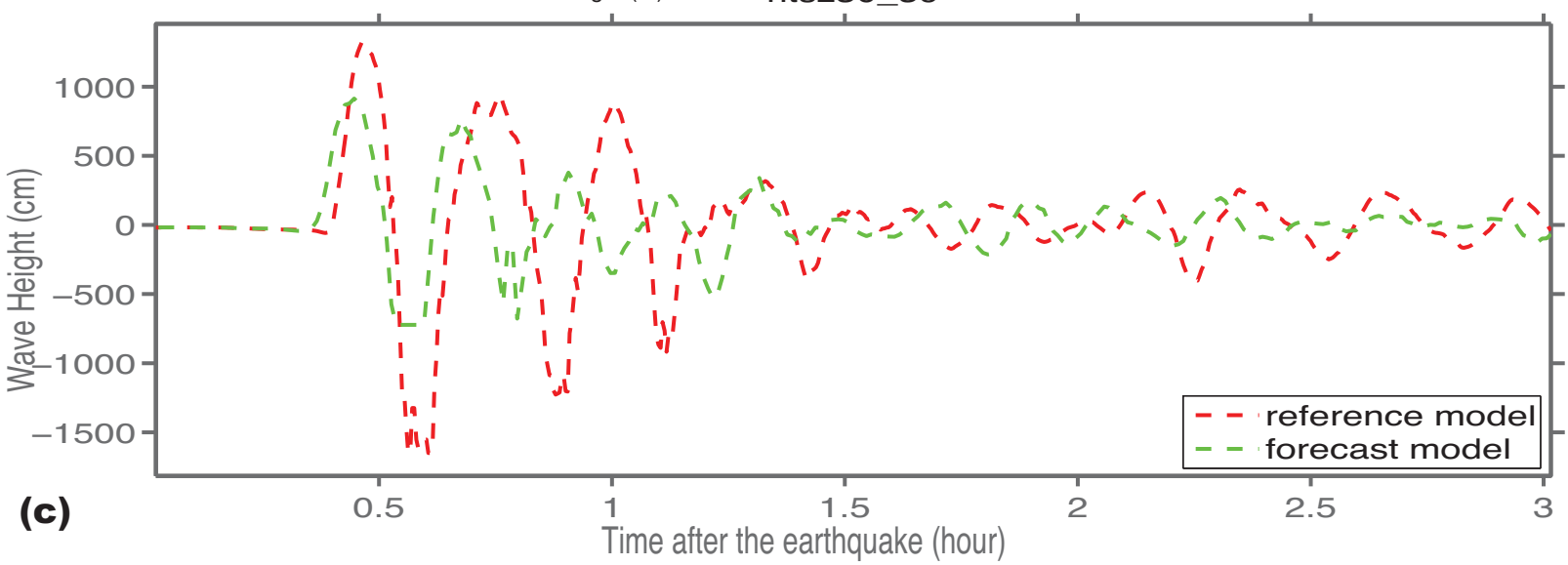
1000
500
0
−500
−1000
−1500
Wave Height (cm)
0.5
1
1.5
2
2.5
3
Time after the earthquake (hour)
reference model
forecast model
(c)

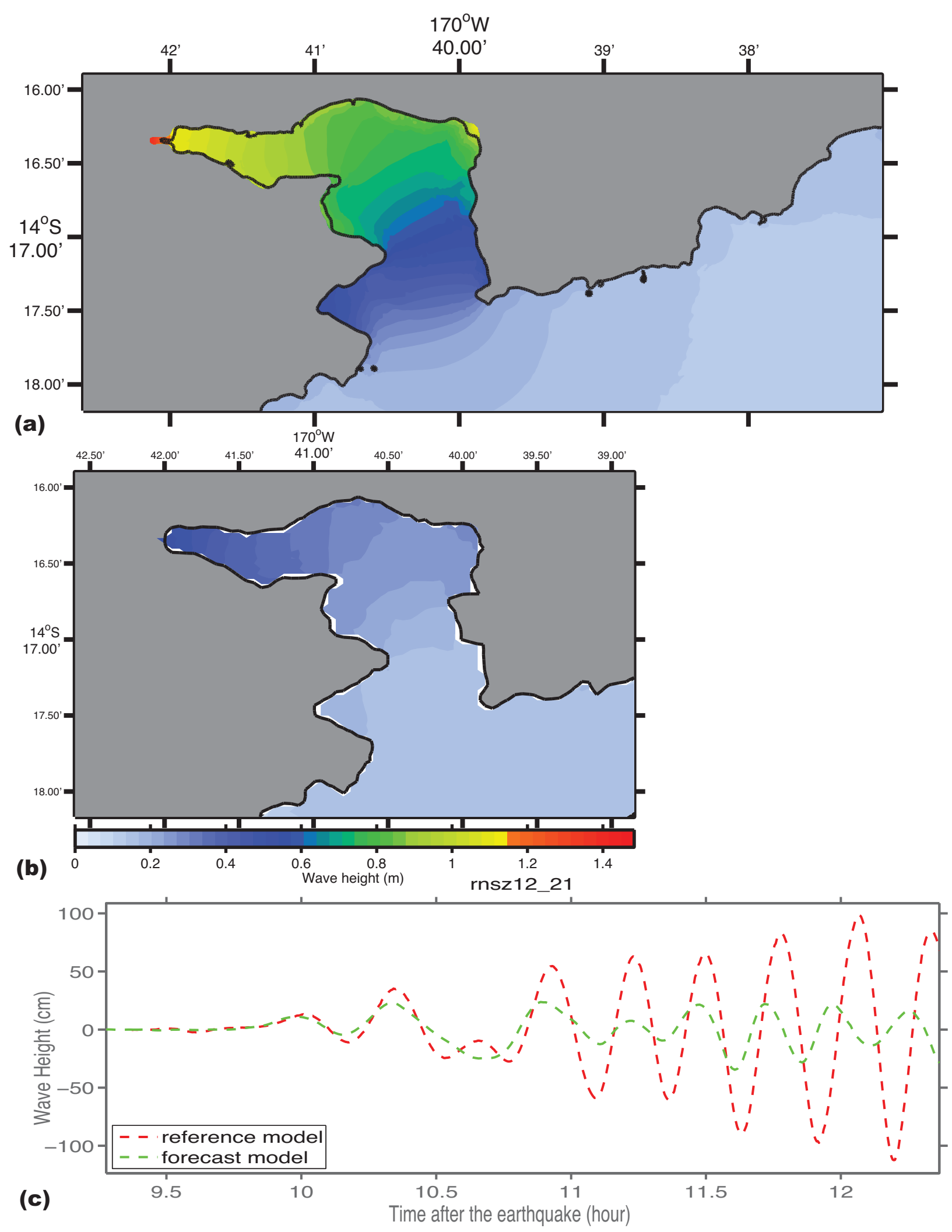
170°W
40.00'
42'
41'
39'
38'
16.00'
16.50'
14°S
17.00'
17.50'
18.00'
(a)
170°W
41.00'
42.50'
42.00'
41.50'
40.50'
40.00'
39.50'
39.00'
16.00'
16.50'
14°S
17.00'
17.50'
18.00'
0
0.2
0.4
0.6
0.8
1
1.2
1.4
Wave height (m)
(b)
rnsz12_21
100
50
0
−50
−100
Wave Height (cm)
reference model
forecast model
9.5
10
10.5
11
11.5
12
Time after the earthquake (hour)
(c)

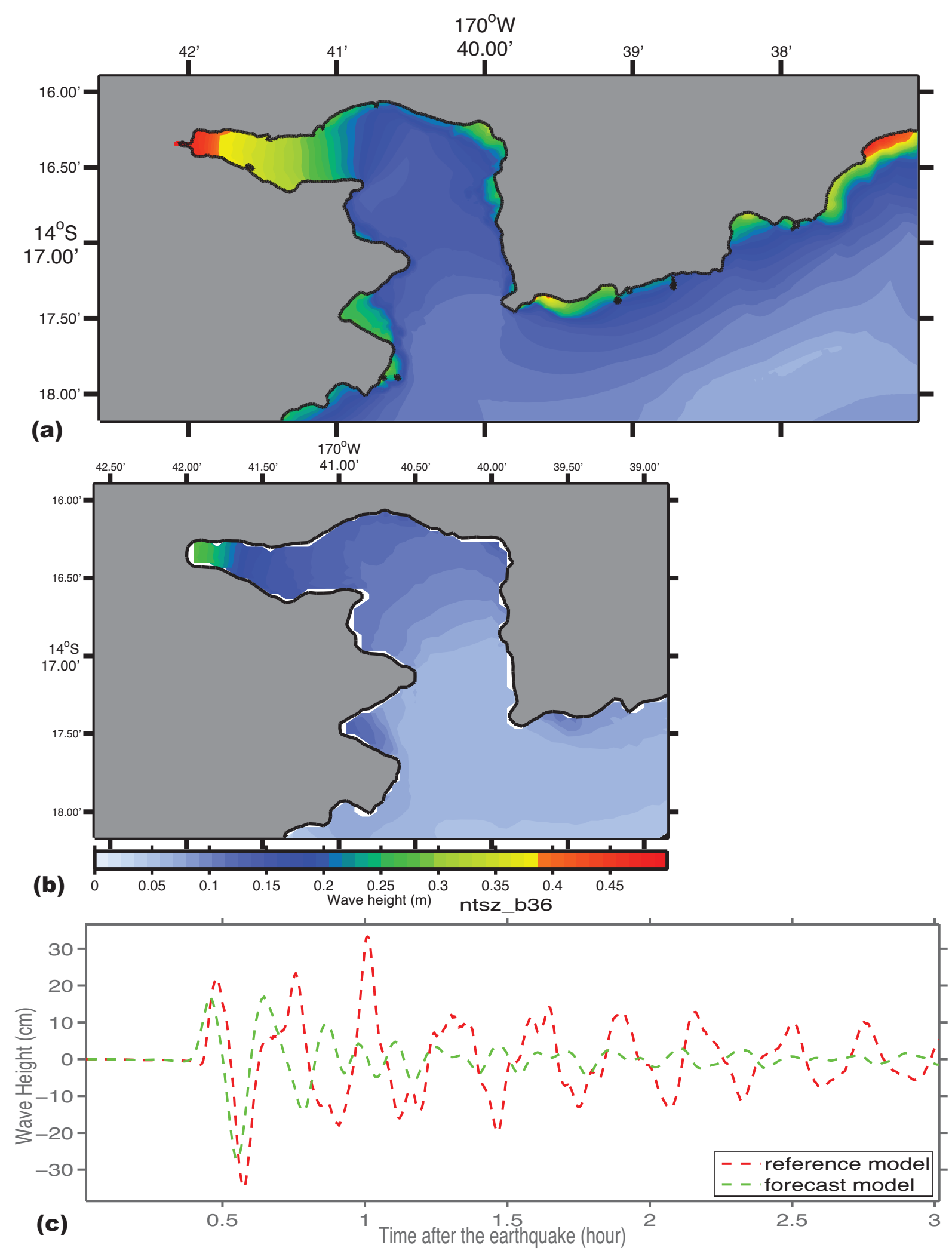
170°W
40.00'
42'
41'
39'
38'
16.00'
16.50'
14°S
17.00'
17.50'
18.00'
(a)
170°W
41.00'
42.50'
42.00'
41.50'
40.50'
40.00'
39.50'
39.00'
16.00'
16.50'
14°S
17.00'
17.50'
18.00'
(b)
0
0.05
0.1
0.15
0.2
0.25
0.3
0.35
0.4
0.45
Wave height (m)
ntsz_b36
Wave Height (cm)
30
20
10
0
−10
−20
−30
reference model
forecast model
(c)
0.5
1
1.5
2
2.5
3
Time after the earthquake (hour)

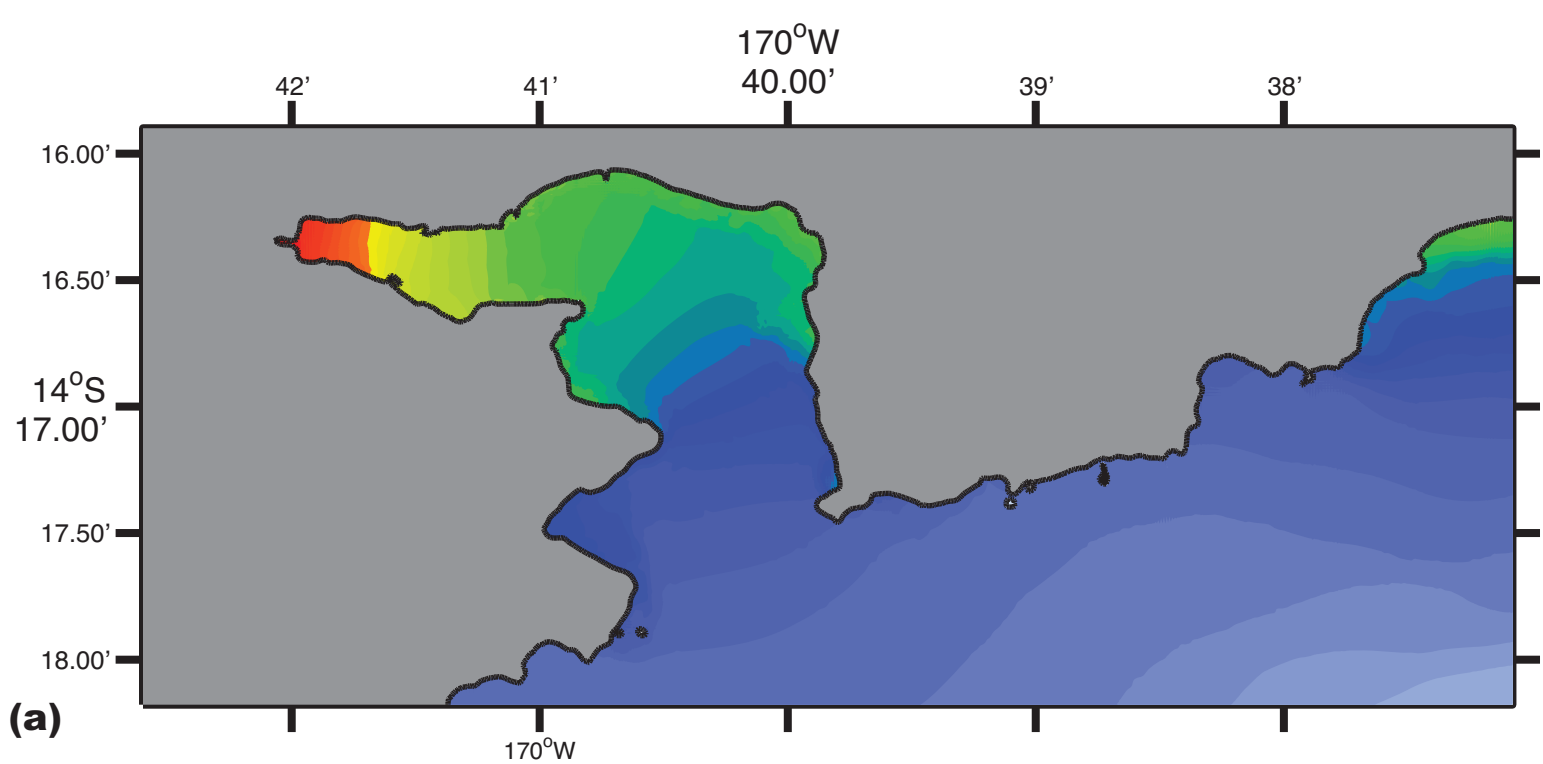
170°W
40.00'
42'
41'
39'
38'
16.00'
16.50'
14°S
17.00'
17.50'
18.00'

(a)

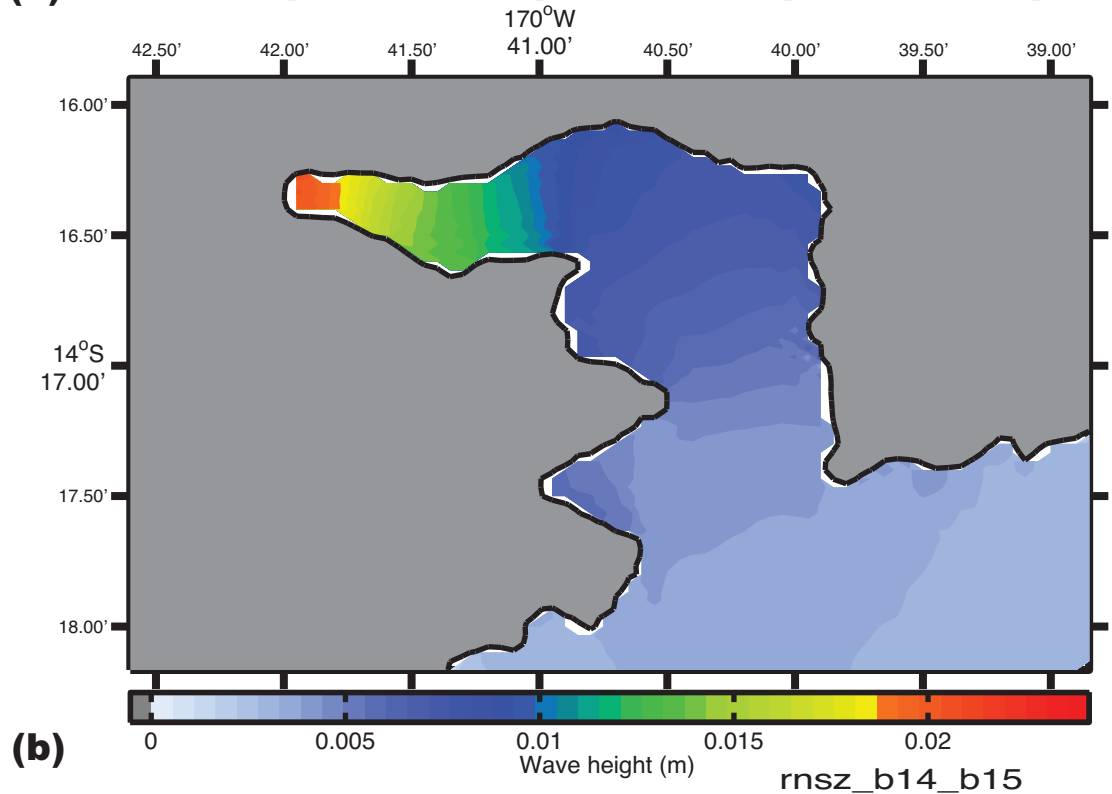
170°W
41.00'
42.50'
42.00'
41.50'
40.50'
40.00'
39.50'
39.00'
16.00'
16.50'
14°S
17.00'
17.50'
18.00'
0
0.005
0.01
0.015
0.02
Wave height (m)

(b)

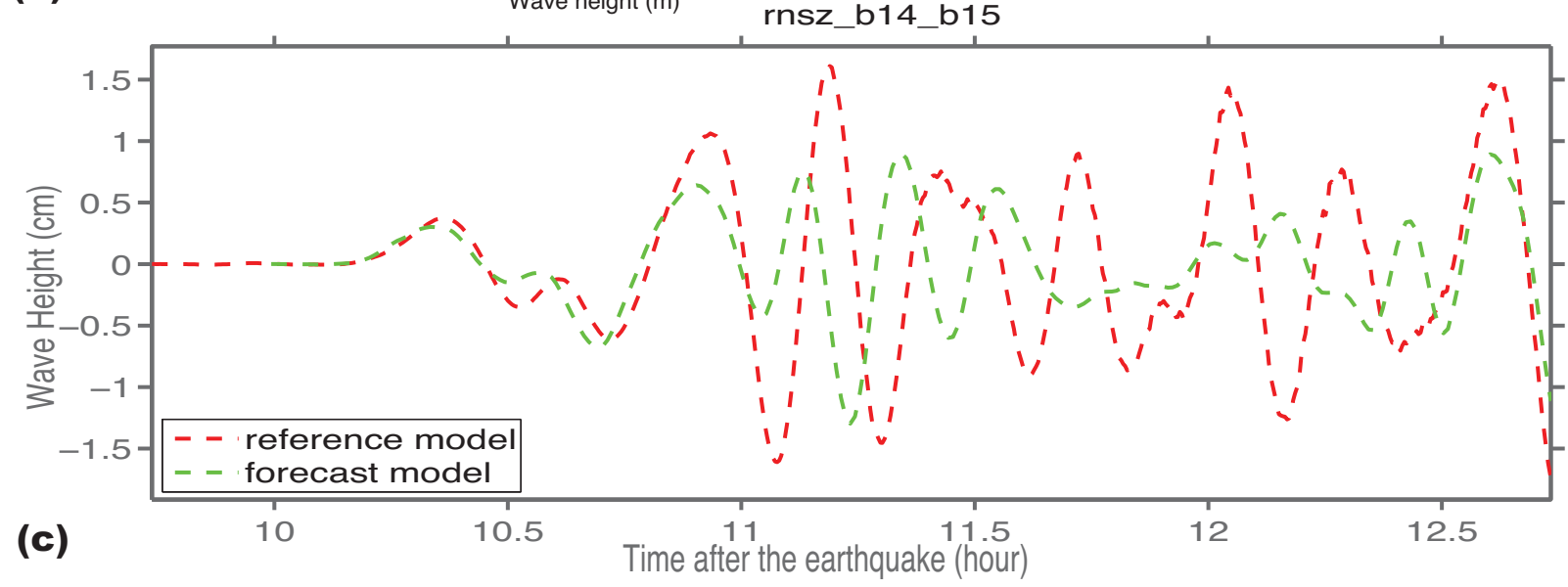
rnsz_b14_b15
1.5
1
0.5
0
−0.5
−1
−1.5
Wave Height (cm)
reference model
forecast model
10
10.5
11
11.5
12
12.5
Time after the earthquake (hour)

(c)

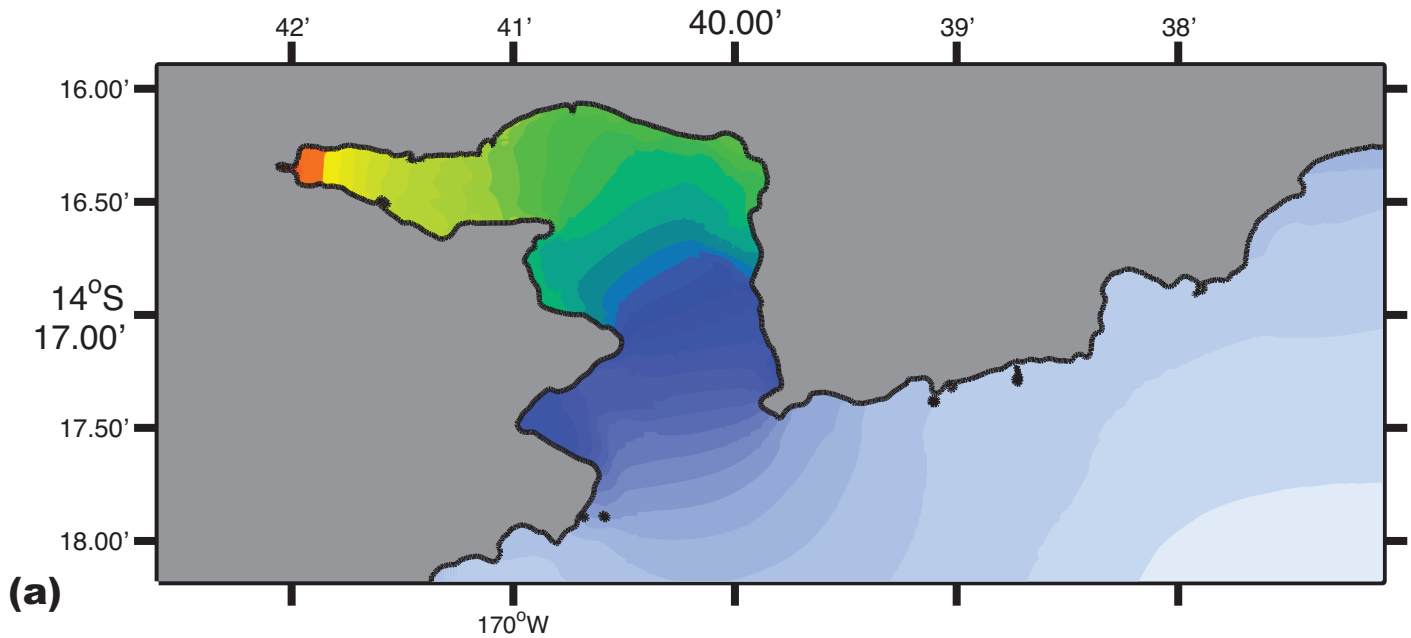
42’
41’
40.00’
39’
38’
16.00’
16.50’
14°S
17.00’
17.50’
18.00’
(a)

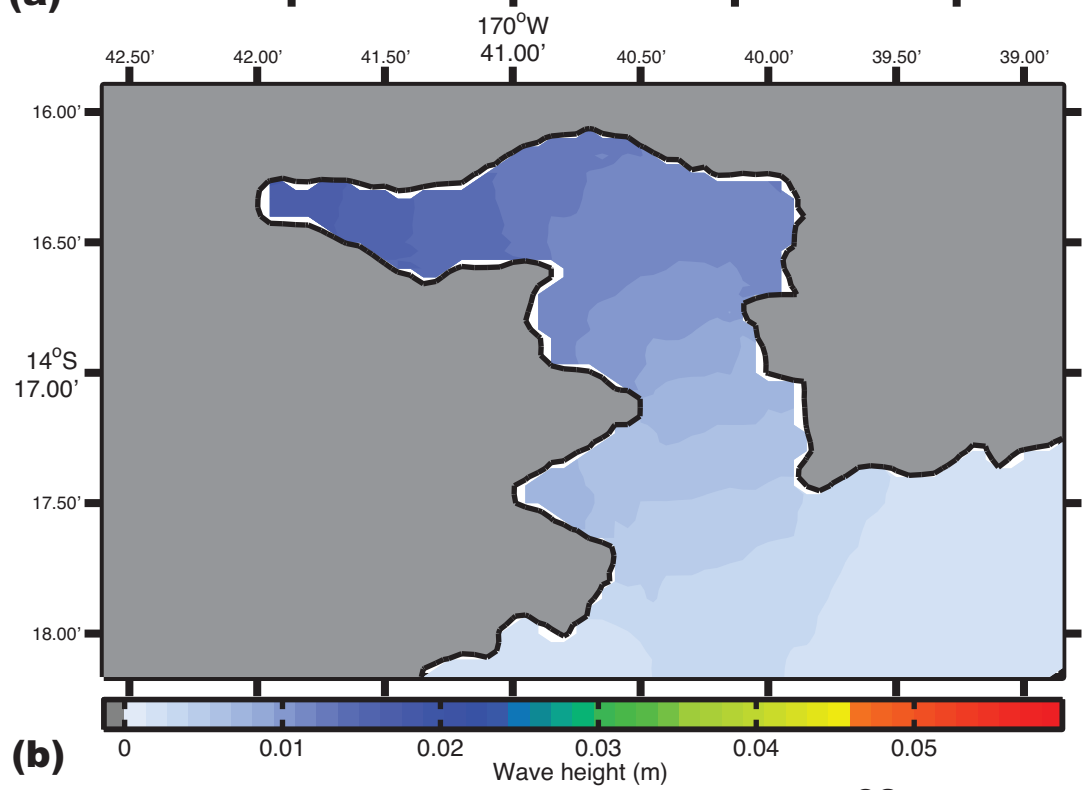
170°W
41.00’
42.50’
42.00’
41.50’
40.50’
40.00’
39.50’
39.00’
16.00’
16.50’
14°S
17.00’
17.50’
18.00’
0
0.01
0.02
0.03
0.04
0.05
Wave height (m)
(b)

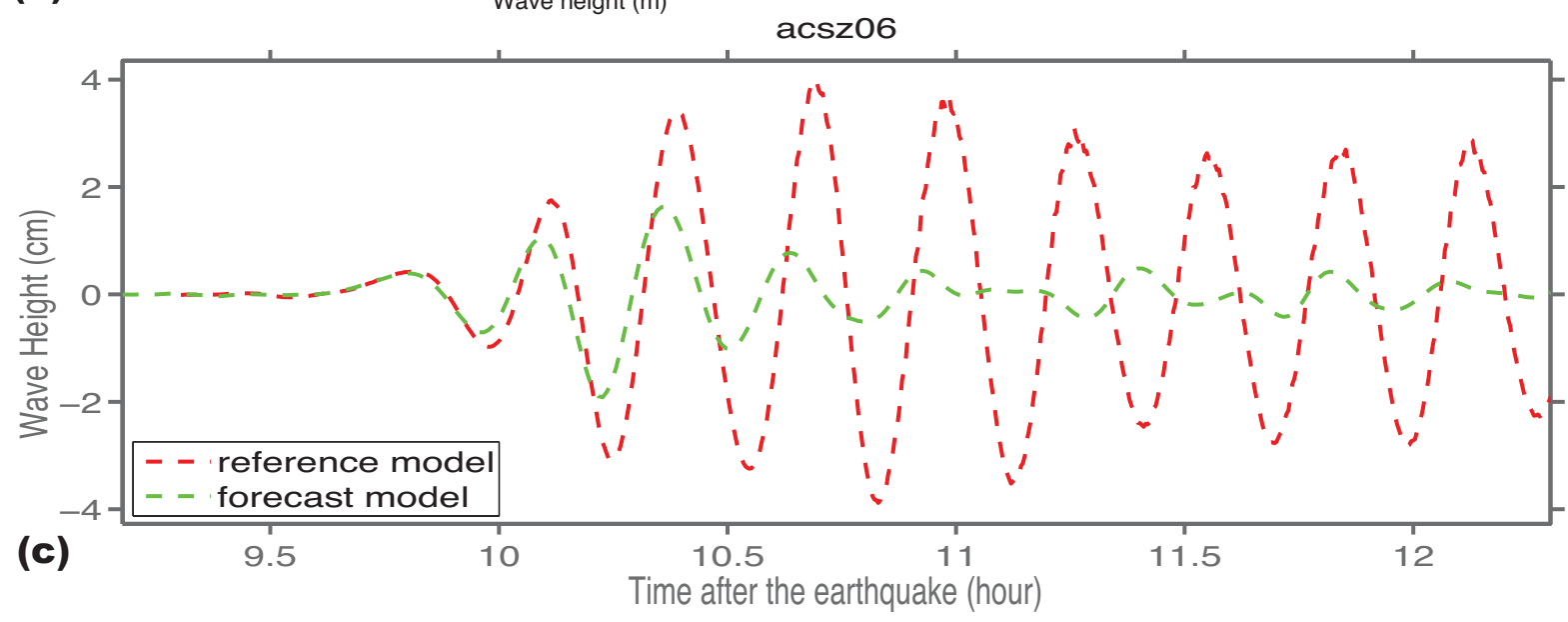
acsz06
4
2
0
−2
−4
Wave Height (cm)
reference model
forecast model
9.5
10
10.5
11
11.5
12
Time after the earthquake (hour)
(c)

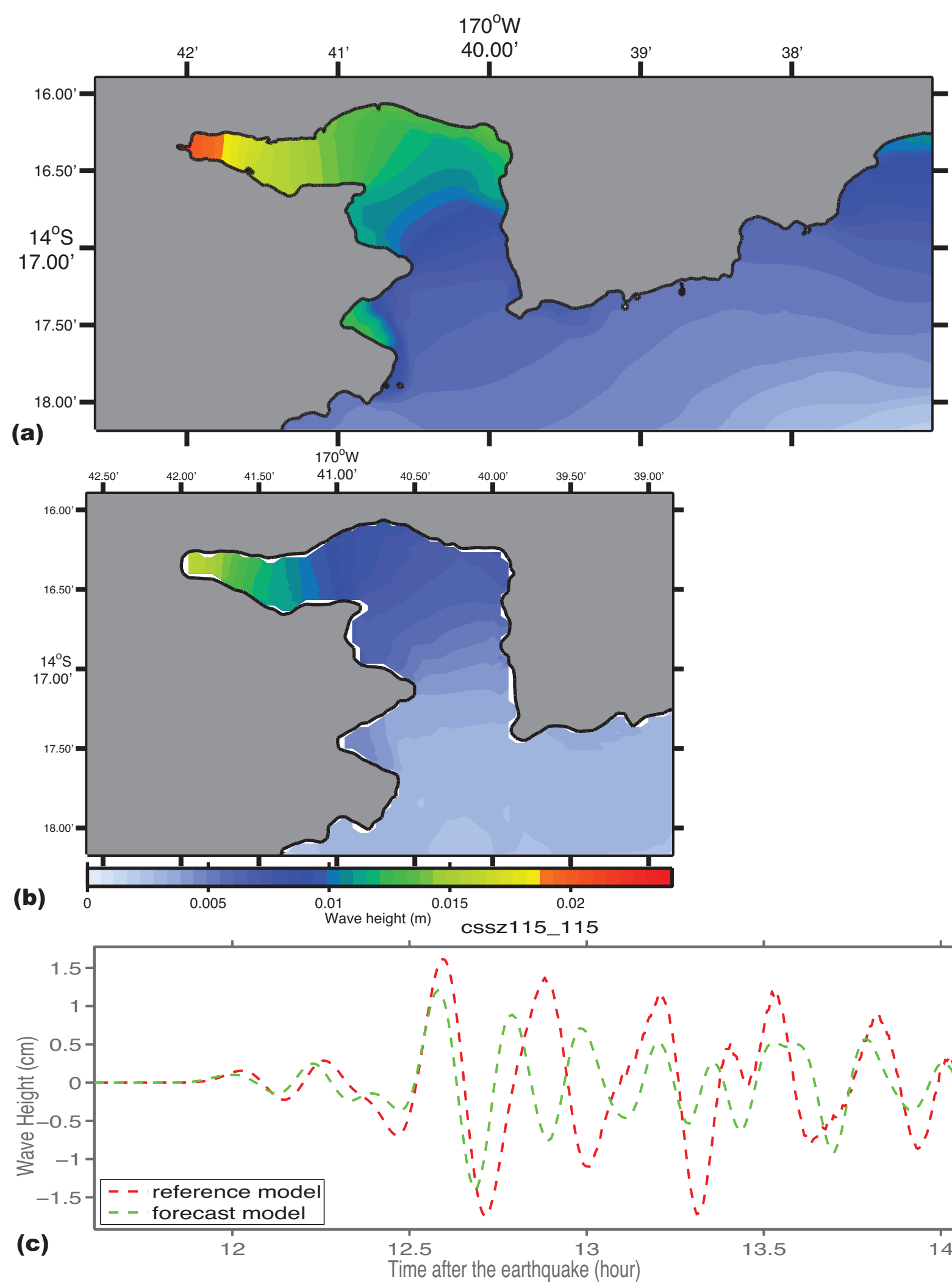
170°W
40.00'
42'
41'
39'
38'
16.00'
16.50'
14°S
17.00'
17.50'
18.00'
(a)
170°W
41.00'
42.50'
42.00'
41.50'
40.50'
40.00'
39.50'
39.00'
16.00'
16.50'
14°S
17.00'
17.50'
18.00'
0
0.005
0.01
0.015
0.02
Wave height (m)
(b)
cssz115_115
1.5
1
0.5
0
−0.5
−1
−1.5
Wave Height (cm)
reference model
forecast model
12
12.5
13
13.5
14
Time after the earthquake (hour)
(c)

Appendix A

Development of the Pago Pago, American Samoa tsunami forecast model occurred prior to parameter changes that were made to reflect modifications to the MOST model code. As a result, the input file for running both the optimized tsunami forecast model and the high-resolution reference inundation model in MOST have been updated accordingly. Appendix A1 and A2 provide the updated files for Pago Pago, American Samoa.

A1. RIM*.infile for Pago Pago, American Samoa

0.0001	Minimum amplitude of input offshore wave (m)
0	Input minimum depth for offshore (m)
0.1	Input "dry land" depth for inundation (m)
0.001	Input friction coefficient (n**2)
1	A & B-grid runup flag (0=disallow, 1=allow runup)
1000.0	Blow-up limit (maximum eta before blow-up)
0.15	Input time step (sec)
72000	Input number of steps
8	Compute "A" arrays every n^{th} time step, n=
1	Compute "B" arrays every n^{th} time step, n=
104	Input number of steps between snapshots
0	...Starting from
1	...Saving grid every n^{th} node, n=1

A2. SIM*.infile for Pago Pago, American Samoa

0.001	Minimum amplitude of input offshore wave (m)
10	Input minimum depth for offshore (m)
0.1	Input "dry land" depth for inundation (m)
0.001	Input friction coefficient (n**2)
1	A & B-grid runup flag (0=disallow, 1=allow runup)
100.0	Blow-up limit (maximum eta before blow-up)
1.5	Input time step (sec)
19200	Input number of steps
2	Compute "A" arrays every n^{th} time step, n=
1	Compute "B" arrays every n^{th} time step, n=
24	Input number of steps between snapshots
0	...Starting from
1	...Saving grid every n^{th} node, n=1